

Efficient formation of a massive quiescent galaxy at redshift 4.9 Graaff, A.G. de; Setton, D.J.; Brammer, G.; Cutler, S.; Suess, K.A.; Labbé, I.; ...; Williams, C.C.

### Citation

Graaff, A. G. de, Setton, D. J., Brammer, G., Cutler, S., Suess, K. A., Labbé, I., ... Williams, C. C. (2024). Efficient formation of a massive quiescent galaxy at redshift 4.9. *Nature Astronomy*. doi:10.1038/s41550-024-02424-3

Version: Accepted Manuscript

License: <u>Leiden University Non-exclusive license</u>

Downloaded from: <a href="https://hdl.handle.net/1887/4179804">https://hdl.handle.net/1887/4179804</a>

**Note:** To cite this publication please use the final published version (if applicable).

# Efficient formation of a massive quiescent galaxy at redshift 4.9

Anna de Graaff<sup>1\*</sup>, David J. Setton<sup>2,3</sup>, Gabriel Brammer<sup>4</sup>, Sam Cutler<sup>5</sup>, Katherine A. Suess<sup>6,7</sup>, Ivo Labbé<sup>8</sup>, Joel Leja<sup>9</sup>, Andrea Weibel<sup>10</sup>, Michael V. Maseda<sup>11</sup>, Katherine E. Whitaker<sup>5,4</sup> Rachel Bezanson<sup>12</sup>, Leindert A. Boogaard<sup>1</sup>, Nikko J. Cleri<sup>13,14</sup>, Gabriella De Lucia<sup>15</sup>, Marijn Franx<sup>16</sup>, Jenny E. Greene<sup>2</sup>, Michaela Hirschmann<sup>17,15</sup>, Jorryt Matthee<sup>18</sup>, Ian McConachie<sup>19</sup>, Rohan P. Naidu<sup>20</sup>, Pascal A. Oesch<sup>10,4</sup>, Sedona H. Price<sup>12</sup>, Hans-Walter Rix<sup>1</sup>, Francesco Valentino<sup>21</sup>, Bingjie Wang<sup>9</sup>, Christina C. Williams<sup>22</sup>

<sup>&</sup>lt;sup>1\*</sup>Max Planck Institute for Astronomy, Königstuhl 17, Heidelberg, 69117, Germany. <sup>2</sup>Department of Astrophysical Sciences, Princeton University, 4 Ivy Lane, Princeton, 08544, New Jersey, United States.

<sup>3</sup>Brinson Prize Fellow.

<sup>&</sup>lt;sup>4</sup>Cosmic Dawn Center, University of Copenhagen, Jagtvej 128, Copenhagen N 2200, Denmark.

<sup>&</sup>lt;sup>5</sup>Department of Astronomy, University of Massachusetts, Amherst, MA 01003, USA. <sup>6</sup>Kavli Institute for Particle Astrophysics and Cosmology and Department of Physics, Stanford University, 452 Lomita Mall, Stanford, 94305, USA. <sup>7</sup>NHFP Hubble Fellow.

<sup>&</sup>lt;sup>8</sup>Centre for Astrophysics and Supercomputing, Swinburne University of Technology, Melbourne, VIC 3122, Australia.

 $<sup>^{9}</sup>$  Department of Astronomy & Astrophysics, The Pennsylvania State University , University Park, 16802, USA.

<sup>&</sup>lt;sup>10</sup>Department of Astronomy, University of Geneva, Chemin Pegasi 51, Versoix, 1290, GE. Switzerland.

<sup>&</sup>lt;sup>11</sup>Department of Astronomy, University of Wisconsin-Madison, 475 N. Charter St., Madison, 53706, Wisconsin, United States.

<sup>&</sup>lt;sup>12</sup>Department of Physics and Astronomy and PITT PACC, University of Pittsburgh, Pittsburgh, PA, 15260, USA.

 $<sup>^{13}\</sup>mathrm{Department}$  of Physics and Astronomy, Texas A&M University, College Station, TX, 77843-4242 USA.

<sup>&</sup>lt;sup>14</sup>George P. and Cynthia Woods Mitchell Institute for Fundamental Physics and Astronomy, Texas A&M University, College Station, TX, 77843-4242 USA.

<sup>&</sup>lt;sup>15</sup>INAF - Astronomical Observatory of Trieste, via G.B. Tiepolo 11, Trieste, 34143,

- <sup>16</sup>Leiden Observatory, Leiden University, P.O.Box 9513, NL-2300 AA Leiden, The Netherlands.
- <sup>17</sup>Institute for Physics, GalSpec laboratory, EPFL, Observatory of Sauverny, Chemin Pegasi 51, Versoix, 1290, Switzerland.
  - <sup>18</sup>Institute of Science and Technology Austria (ISTA), Amp Campus 1, Klosterneuburg, 3400, Austria.
- <sup>19</sup>Department of Physics & Astronomy, University of California Riverside, Riverside, 92521, USA.
- <sup>20</sup>MIT Kavli Institute for Astrophysics and Space Research, 77 Massachusetts Ave., Cambridge, 02139, USA.
- <sup>21</sup>European Southern Observatory, Karl-Schwarzschild-Str. 2, Garching bei München, 85748, Germany.
  - <sup>22</sup>NSF's National Optical-Infrared Astronomy Research Laboratory, 950 North Cherry Avenue, Tucson, AZ 85719, USA.

\*Corresponding author(s). E-mail(s): degraaff@mpia.de;

#### Abstract

Within the established framework of structure formation, galaxies start as systems of low stellar mass and gradually grow into far more massive galaxies [1, 2]. The existence of massive galaxies in the first billion years of the Universe, suggested by recent observations, appears to challenge this model, as such galaxies would require highly efficient conversion of baryons into stars[3-6]. An even greater challenge in this epoch is the existence of massive galaxies that have already ceased forming stars [7-9]. However, robust detections of early massive quiescent galaxies have been challenging due to the coarse wavelength sampling of photometric surveys. Here we report the spectroscopic confirmation with the James Webb Space Telescope of the quiescent galaxy RUBIES-EGS-QG-1 at redshift z = 4.90, 1.2 billion years after the Big Bang. Deep stellar absorption features in the spectrum reveal that the galaxy's stellar mass of  $10^{11} M_{\odot}$  formed in a short 200 Myr burst of star formation, after which star formation activity dropped rapidly and persistently. According to current galaxy formation models, systems with such rapid stellar mass growth and early quenching are too rare to plausibly occur in the small area probed spectroscopically with JWST. Instead, the discovery of RUBIES-EGS-QG-1 implies that early massive quiescent galaxies can be quenched earlier or exhaust gas available for star formation more efficiently than currently assumed.

RUBIES-EGS-QG-1 was identified as a candidate massive quiescent galaxy at z > 4.5 based on its red color measured from photometry across 1–5  $\mu$ m in the Extended Groth Strip (EGS) obtained with the NIRCam instrument of the James Webb Space Telescope (JWST) [10–12]. The source was subsequently selected as a target for spectroscopic follow-up with JWST/NIRSpec because of its red color, F150W – F444W =

2.35, and bright apparent magnitude at long wavelengths, F444W = 22.5. The low-resolution PRISM spectrum of RUBIES-EGS-QG-1 obtained with JWST/NIRSpec (Figure 1) reveals deep Balmer absorption lines and a strong spectral break at a rest-frame wavelength of 4000  $\mathring{A}$ , indicating a lack of star formation in its recent history.

We detect the [O III] $_{\lambda\lambda4960,5008}$ , [S II] $_{\lambda\lambda6718,6733}$  and blended H $\alpha$  and [N II] $_{\lambda\lambda6549,6585}$  emission lines in the PRISM spectrum. A grating spectrum of RUBIES-EGS-QG-1 with higher spectral resolution across 2.9–5.2  $\mu$ m reveals weak H $\alpha$  emission infilling the stellar absorption feature and strong [N II] emission at a redshift of  $z=4.8976\pm^{0.0006}_{0.0010}$  (see Methods). A marginal detection of H $\alpha$  implies log [N II] $_{\lambda6585}$ /H $\alpha\approx0.5$  and exceeds the ratio that can be explained by photoionization from massive stars by a factor  $\approx 3[13]$ . Therefore, the emission lines do not appear to be connected to ongoing star formation activity, but rather suggest the presence of an active galactic nucleus (AGN), although we cannot rule out the presence of shocked gas[14]. Despite evidence for an AGN, the deep Balmer lines, indicative of a post-starburst system[15], suggest that the continuum emission of the spectrum is dominated by an evolved stellar population.

The high redshift of RUBIES-EGS-QG-1 allows for stringent constraints on its star formation history in the first billion years of the Universe. To measure the star formation history, we use Prospector [16] to jointly fit a 21-parameter model to the PRISM spectrum and the observed photometry from the Hubble Space Telescope (HST) and JWST (see Methods for a complete description). In brief, the model star formation history is parameterized as 14 time bins of constant star formation, with a common metallicity, dust attenuation, intrinsic velocity dispersion, and stellar initial mass function (IMF). We fit nebular emission lines using a simple model where lines are approximated by Gaussian profiles but no assumption is made on the origin of the emission, and utilize a 6th-order polynomial to account for uncertainty in the flux calibration of the spectrum. We explore the effect of deviations in choices from our fiducial model in the Methods.

The median model of the sampled posterior is shown in red in Figure 1. We find a high stellar mass of  $9.9 \pm ^{0.4}_{0.5} \times 10^{10}\,\rm M_{\odot}$ , and a low star formation rate in the past  $100~\rm Myr, SFR_{100} = 4.0 \pm ^{3.5}_{1.0}\,\rm M_{\odot}\,yr^{-1}$ . Together, these correspond to a low specific star formation rate of sSFR = 4.0

 ${\rm pm}_{0.8}^{1.0} \times 10^{-11} \, {\rm yr}^{-1}$  cementing RUBIES-EGS-QG-1 as the highest-redshift spectroscopic confirmation of a massive quiescent galaxy to date. We infer low attenuation by dust, with the V-band attenuation from our modeling  $A_{\rm v} = 0.17 \pm_{0.05}^{0.06}$ . The spectrum unambiguously demonstrates the red rest-frame optical color is dominated by old stars rather than dust-obscured star formation. This is corroborated by a non-detection in NOEMA observations at 1.1 mm, which implies a  $3\sigma$  upper limit on the dust-obscured star formation rate of  $120 \, {\rm M}_{\odot} \, {\rm yr}^{-1}$ .

We show the resulting star formation history of the galaxy in the top panel of Figure 2 in purple. RUBIES-EGS-QG-1 assembled its stellar mass within a short burst of star formation, of  $\Delta t = 180 \pm_{10}^{170}$  Myr, that peaked at a star formation rate of SFR<sub>peak</sub> =  $870 \pm_{140}^{70}$  M<sub>☉</sub> yr<sup>-1</sup>. For our fiducial model, half of the stellar mass was formed in the first  $t_{\rm form} = 480 \pm_{10}^{30}$  Myr of cosmic time, which would mark it as one of

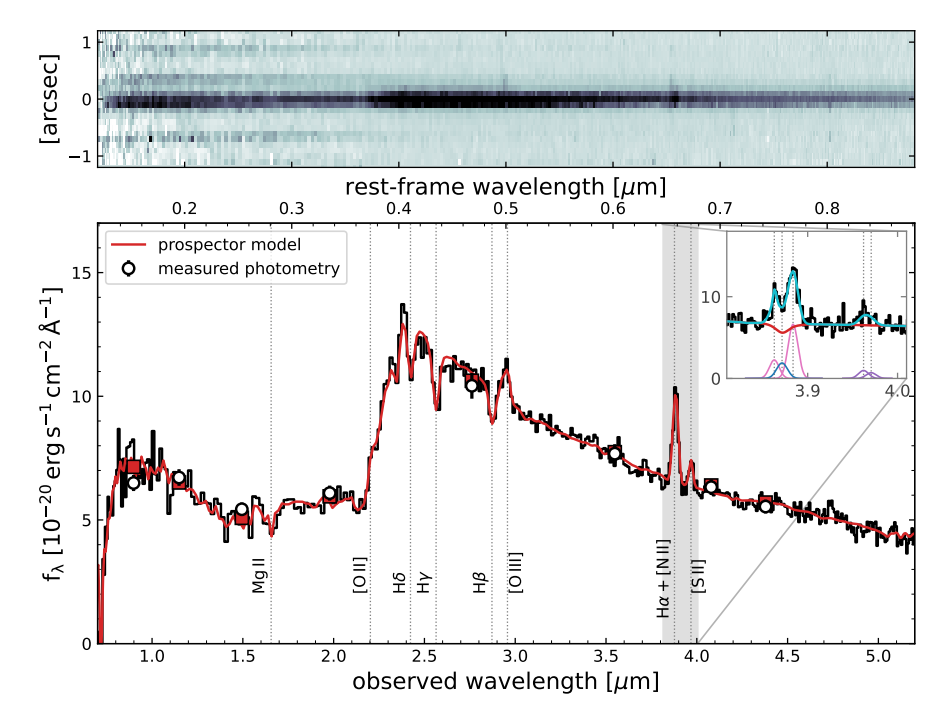


Fig. 1 JWST/NIRSpec PRISM spectrum of the massive quiescent galaxy RUBIES-EGS-QG-1 at a redshift of z=4.8976. The inset shows the medium-resolution (NIRSpec G395M) spectrum around the wavelength of H $\alpha$ . Both spectra were calibrated to the measured photometry using Prospector . The spectrum shows deep Balmer absorption lines, similar to post-starburst galaxies at lower redshifts, and implies a lack of star formation in its recent history. The presence of the emission line doublets [O III], [N II], [S II], and the minimal inferred infilling of the H $\alpha$  absorption line are consistent with AGN activity.

the earliest-forming massive galaxies observed. We measure a corresponding quenching timescale  $t_{90}-t_{\rm form}=100\pm^{10}_{10}$  Myr, indicating that the decline in star formation from its peak in RUBIES-EGS-QG-1 was extremely rapid.

Crucially, we find that the inferred stellar mass, the duration of the star formation burst, and the lack of recent star formation activity are largely robust against choices made in the model parameterization and star formation history priors. A full description of models tested can be found in the Methods. However, we find that the age of the stellar population depends strongly on the assumed metallicity of the system. Our fiducial fit with the metallicity as free parameter indicates a low stellar metallicity ( $\approx 0.2\,Z_\odot$ ), and an old stellar population that formed as early as  $z_{\rm form}=10.0\pm_{0.2}^{0.4}$  and stopped growing by  $z\approx 8.6$ . Recent work has shown that the elemental abundance patterns in high-redshift quiescent galaxies differ from the solar abundance patterns typically used in stellar population modeling, which can lead to incorrectly inferred stellar metallicities [17]. If we instead fix the metallicity of the stellar population to the solar value, we infer a substantially younger population with a formation redshift of  $z_{\rm form}=6.3\pm_{0.2}^{0.1}$  as well as more recent quenching (shown as the blue curve on Figure

2). Although we cannot robustly differentiate between these two star formation histories with our current data, we stress that the stellar mass, the timescale and peak of the burst of star formation and quenching timescale do not depend significantly on metallicity.

We estimate the dynamical mass of the system using the observed widths of the emission lines and the half-light radius measured from the F444W image,  $r_{\rm e}=0.55\pm0.01\,{\rm kpc}$  (rest-frame wavelength of 0.75  $\mu{\rm m}$ ; see Methods): we find that  ${\rm M_{dyn}}=2.7\pm^{0.7}_{0.8}\times10^{11}\,{\rm M_{\odot}}$  is consistent with RUBIES-EGS-QG-1 being a very massive galaxy. The dynamical mass is a factor 3 higher than the stellar mass estimate, although we note that the estimated dynamical mass may be elevated by a factor 2-3 due to non-gravitational motions of the ionized gas that we have not accounted for. As the centers of high-redshift massive galaxies are expected to be dominated by stellar mass within the effective radius[18], this suggests that the stellar mass is not substantially underor overestimated, despite uncertainties in the IMF assumed in our modeling.

The stellar mass surface density within the estimated half-light radius of  $\Sigma_*(< r_{\rm e}) = 5.2^{+0.2}_{-0.3} \times 10^{10}\,{\rm M_{\odot}}\,{\rm kpc}^{-2}$  is high, but well within theoretical limits for the maximum surface density achievable in a short burst of star formation[19, 20]. It is also in line with previous work at z < 3 which demonstrated a strong link between low specific star formation rates and high central mass densities, with a threshold density for quiescence that increases toward higher redshift[21, 22]. This connection between galaxy structure and the star formation history has been interpreted as a compaction event followed by quenching due to feedback from intense star formation and an AGN[23], and is consistent with the high [N II]/H $\alpha$  ratio observed in RUBIES-EGS-QG-1 that is indicative of an AGN or shocked gas.

With a peak star formation rate of  $\approx 870 \,\mathrm{M}_{\odot} \,\mathrm{yr}^{-1}$  at z > 6, RUBIES-EGS-QG-1 had a higher star formation activity than a large sample of the 40 most UV-luminous sources at  $z \sim 7$  discovered over an area of 7 degree<sup>2</sup>[24]. Interestingly, the star formation rate and its star formation rate surface density  $(\Sigma_{SFR} \approx 450 \,\mathrm{M}_{\odot} \,\mathrm{yr}^{-1} \,\mathrm{kpc}^{-2})$ are similar to the properties of the dusty star-forming galaxy G09 83808 at  $z \approx 6$  that resembles a local ultra-luminous infrared galaxy [25] and the submillimeter galaxy SPT0311-58 at z = 6.9 [26]. The star formation history of RUBIES-EGS-QG-1 also matches well with the inferred star formation histories of the brightest red sources found with JWST [27] at  $z \sim 7$ , provided that the light emitted by these sources originates from stars. These different observations suggest that the burst of star formation that formed RUBIES-EGS-QG-1 could too have been strongly dust-obscured. Such a link has also been suggested for the other spectroscopically-confirmed massive quiescent galaxy at z > 4.5 [9], observed at z = 4.658 with a stellar mass of  $\approx 3.8 \times 10^{10} \,\mathrm{M_{\odot}}$  formed at  $z_{\mathrm{form}} = 6.9 \pm 0.2$ . In comparison with this source, however, RUBIES-EGS-QG-1 stands out for being more than twice as massive. On the other hand, a dust-obscured period of star formation may be difficult to reconcile with the inferred low metallicity and the fact that to date no submillimeter galaxy has been found at z>8 with a star formation rate  $>200\,{\rm M}_{\odot}\,{\rm yr}^{-1}[24,\,28]$ . Therefore, this could instead also imply that RUBIES-EGS-QG-1 is an exceptionally rare source, or that the star formation history is either significantly more extended or more bursty than inferred from our modeling. In the latter scenario, finding UV-luminous progenitors

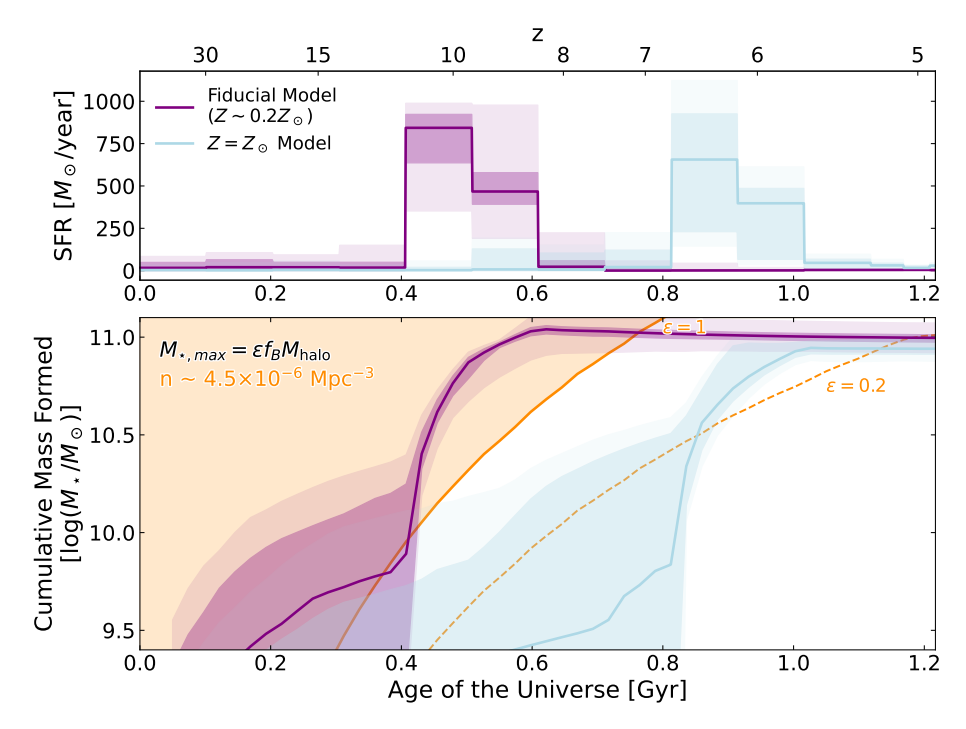


Fig. 2 The history of stellar mass growth in RUBIES-EGS-QG-1. Top: Star formation history inferred from the modeling to the PRISM spectrum and photometry for the fiducial (free-metallicity) model (purple) and the fixed-solar metallicity model (blue). Dark (light) shaded regions indicate the  $1\sigma$  ( $2\sigma$ ) confidence intervals of the posterior distributions. Bottom: The cumulative mass history inferred from the star formation history of the two models. In orange we show the maximum stellar mass formed for a typical halo at the observed number density of massive quiescent galaxies at z>4[10], assuming a universal baryon-to-total matter ratio ( $f_{\rm B}$ ) and different baryon-to-stellar conversion factors ( $\epsilon$ ). This indicates that a short ( $\approx 300\,{\rm Myr}$ ) burst of star formation with high efficiency of  $\epsilon>0.2$  is required to form RUBIES-EGS-QG-1, corresponding to an efficiency at or greater than the peak of the stellar-halo mass relation[29].

at  $z\sim 10$  may be difficult, as the probability of discovery depends on both the low number density of extremely massive high-redshift galaxies and on the duty cycle of star formation.

The mere existence of RUBIES-EGS-QG-1 provides an essential constraint on the growth of the most massive galaxies in the early Universe. In the bottom panel of Figure 2 we show the cumulative mass assembly history of the galaxy derived from the modeled star formation history, subtracting mass returned to the interstellar medium through stellar evolution, as a function of the age of the Universe. The small area targeted with JWST spectroscopy in the RUBIES survey ( $\approx 100\,\mathrm{arcmin^2}$  thus far) implies an observed number density of  $n\approx 3\times 10^{-6}\,\mathrm{Mpc^{-3}}$  at 4.5 < z < 5.5. Based on the photometric selection of candidate massive quiescent galaxies in JWST imaging[10], the comoving number density of quiescent galaxies of similar mass to RUBIES-EGS-QG-1  $(M_*>10^{11}\,\mathrm{M}_\odot)$  is approximately equally low,  $n\approx 4.5\times 10^{-6}\,\mathrm{Mpc^{-3}}$  at 4 < z < 5. We can hence use this number density to estimate the typical dark matter halo mass

at a fixed redshift and derive an approximate limit on the total baryonic mass available within the halo[4]. This can then be converted to a maximum stellar mass at a given redshift by assuming  $M_*(z) = \epsilon f_{\rm B} M_{\rm halo}(z)$ , where  $f_{\rm B}$  is the cosmic baryon fraction (15.6%, [30]) and  $\epsilon$  is the baryon-to-star conversion efficiency. We plot this expected stellar mass for two values of the baryon efficiency:  $\epsilon = 1$  (i.e. assuming total conversion of baryons to stars), and the efficiency at the peak of the stellar-halo mass relation of  $\epsilon = 0.2$ [29]. The cumulative mass assembly history of RUBIES-EGS-QG-1 implies a high efficiency of star formation of  $\epsilon > 0.2$ , and the low-metallicity model even suggests that the galaxy is converting baryons to stars with near-perfect efficiency.

Neither the extremely rapid mass assembly nor the early quenching of RUBIES-EGS-QG-1 are consistent with predictions from large-volume  $(200^3 -$ 800<sup>3</sup> Mpc<sup>3</sup>) cosmological hydrodynamical (FLARES[31], Magneticum Pathfinder[32] and TNG300[33]) and semi-analytic (GAEA[34], SHARK[35]) simulations of galaxy formation. While some of these models are able to produce galaxies that are quiescent at  $z \sim 4.5 - 5.0$  and as massive as RUBIES-EGS-QG-1, such systems are extremely rare: the comoving number densities are approximately  $1-10\times10^{-8}\,\mathrm{Mpc^{-3}}$  in the different simulations, and correspond to very massive haloes. In comparison with the estimated number density of RUBIES-EGS-QG-1, this implies a probability of 1% $(2\sigma \text{ outlier})$  that such a source is observed in the small area probed spectroscopically with JWST ( $\sim 100 \, \mathrm{arcmin^2}$  for the RUBIES program). However, at higher redshifts the comoving number density of quiescent galaxies with stellar masses  $M_* > 10^{11} \,\mathrm{M_{\odot}}$ decreases dramatically, with most simulations containing zero such galaxies at  $z \geq 5$ . The inferred star formation history of RUBIES-EGS-QG-1, where star formation is quenched at  $z \gtrsim 5.5$ , therefore implies that it would be a significant outlier at earlier times.

This indicates that the star formation and feedback recipes in the simulations do not accurately capture the formation and quenching processes of early massive galaxies. Alternatively, to reconcile the formation history of RUBIES-EGS-QG-1 with simulations requires that our estimated observed number density is substantially overestimated, and that the galaxy instead resides in a very rare, and therefore massive, halo ( $M_{\rm halo} \gtrsim 10^{13} \, {\rm M}_{\odot}$  by  $z \sim 5$ ). The effects of cosmic variance may be large for the relatively small area targeted spectroscopically with JWST: although unlikely, it is possible that the observation of RUBIES-EGS-QG-1 is a  $\gtrsim 3\sigma$  chance finding and indeed resides in a very massive halo.

We examine the environment of RUBIES-EGS-QG-1 for evidence of such a large-scale overdensity by compiling all sources in the EGS with robust redshifts from JWST spectroscopy, obtained from a mixture of JWST Cycle 1 and 2 programs using the DAWN JWST Archive (see Methods). In total, we find 6 sources in the direct vicinity of RUBIES-EGS-QG-1 with a redshift separation  $\Delta z < 0.013$  and projected separation of < 1 arcmin (< 2 comoving Mpc), and another 7 sources spread across the field at the same redshift but with larger angular separation (Figure 3). Notably, we find a clustering of 4 sources at a distance of  $\approx$  16 comoving Mpc from RUBIES-EGS-QG-1, of which the brightest galaxy (measured at 4  $\mu$ m) is a sub-millimeter galaxy identified previously in SCUBA-2 data[36]. In comparison with the average density of the

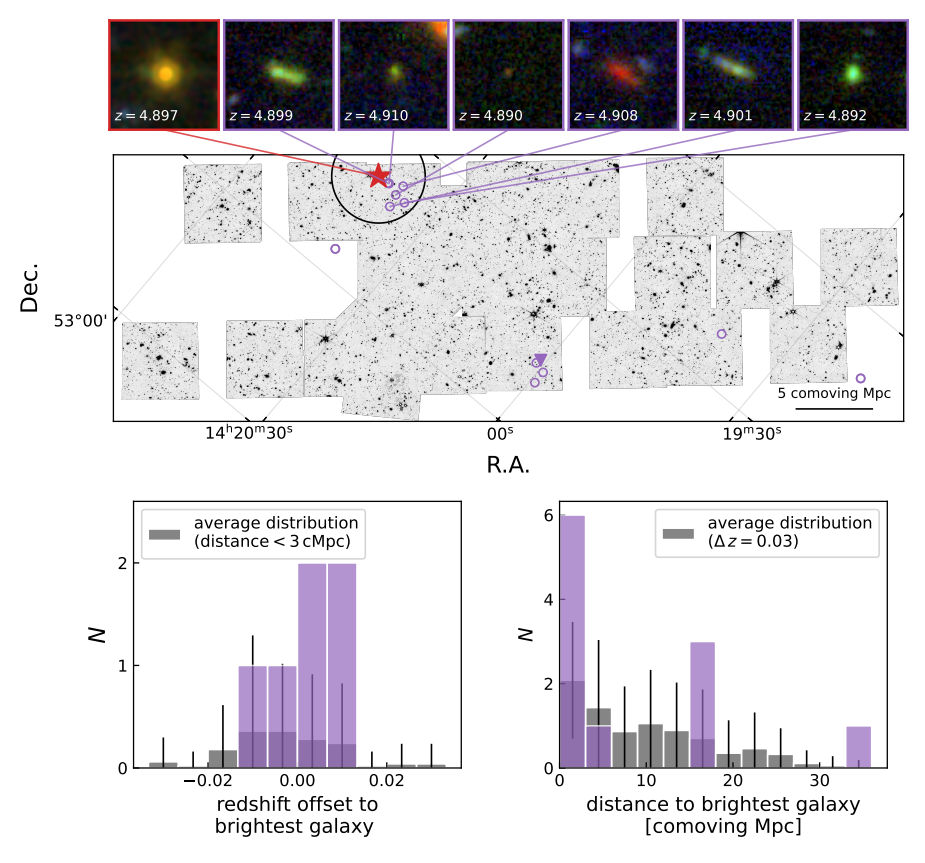


Fig. 3 Spatial clustering of spectroscopically-confirmed sources at  $z\approx 4.90$  (circles) around RUBIES-EGS-QG-1 (red star). The submillimeter galaxy, the brightest source among the group of 4 at a projected distance of 16 comoving Mpc, is indicated by a purple triangle. The background image shows the NIRCam F444W mosaic of the EGS field. Compared to the typical projected spatial clustering (within redshift ranges  $\Delta z=0.03$ ) and redshift clustering (within apertures of radius < 3 Mpc) for galaxies in the redshift range 4 < z<6 with robust redshifts from JWST spectroscopy, RUBIES-EGS-QG-1 clearly resides in an overdense environment, forming the highest redshift known overdensity hosting a massive quiescent galaxy. We show false-color images (created from NIRCam F150W, F277W and F444W images) of RUBIES-EGS-QG-1 and its 6 nearby neighbors.

4 < z < 6 galaxy population, we find clear evidence for an overdensity at z = 4.90 within an aperture of  $\pi \times 3\,\mathrm{Mpc^2}$  (as also suggested in previous literature[37, 38]), forming the highest redshift overdensity containing a massive quiescent galaxy found thus far[39]. However, based on these data alone, we cannot conclusively determine whether the region indeed represents an extremely massive halo, and whether the other 7 sources are associated with the overdensity.

The fact that the galaxy resides in an overdense environment may also point to substantial ex-situ mass accretion, in addition to in-situ star formation. A major merger between two approximately equally massive systems would provide a rapid accretion of stellar mass, allowing for more conventional star formation efficiencies.

Moreover, major mergers have been proposed as a quenching mechanism[40]. However, equal-mass mergers between massive galaxies are exceptionally rare at z > 5, as the simulations predict a number density of  $\lesssim 10^{-8} \, \mathrm{Mpc^{-3}}$  for such systems. We also do not find signatures of recent merging in the morphology of RUBIES-EGS-QG-1 (Figure 3; Methods).

Clearly, the rapid assembly of RUBIES-EGS-QG-1 and its early quenching requires an extreme formation scenario. In the context of recent studies that have reported candidate massive galaxies at z > 6[3] and massive quiescent galaxies with formation times at  $z \gtrsim 6[11, 41-43]$ , RUBIES-EGS-QG-1 stands out for its very high stellar mass, high redshift and deep Balmer absorption features that unambiguously set its formation at z > 6. Although theoretical models can form extremely massive galaxies at early epochs, and some also produce quiescent galaxies at z > 5, the number densities of these sources are extremely low. In the case of RUBIES-EGS-QG-1, this may indicate that the galaxy lies in an extremely rare, massive halo for its redshift, or the exceptional detection of a major merger between two massive galaxies. However, both of these scenarios are expected to be very rare ( $\lesssim 0.1 \text{ per degree}^2$ ), and the area covered by JWST spectroscopy thus far is small. The direct implication of the existence of RUBIES-EGS-QG-1 is therefore that the star formation and feedback prescriptions in theoretical models require revision, as the model universes currently cannot reproduce the stellar mass growth and early quenching required to match the inferred abundance of massive quiescent galaxies.

### Methods

## 1 Spectroscopic data

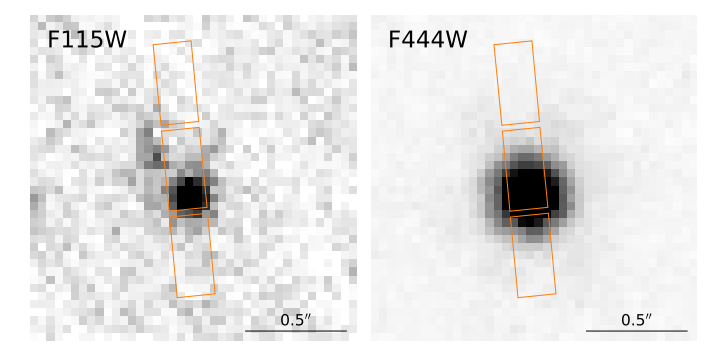
The RUBIES program (GO-4233; PIs A. de Graaff and G. Brammer) is a JWST Cycle 2 program using the NIRSpec microshutter array (MSA)[44] to observe galaxies in the CANDELS EGS and UDS extragalactic deep fields [45, 46]. Specifically, RUBIES targets galaxies detected in F444W from JWST/NIRCam imaging in the Cosmic Evolution Early Release Science (CEERS; program #1345; PI S. Finkelstein) and Public Release IMaging for Extragalactic Research (program #1837; PI J. Dunlop) surveys, and is optimized to reach high spectroscopic completeness for bright and red sources at z > 3. Thus far, the survey has targeted an area of approximately 100 arcmin<sup>2</sup>. Details about the target selection and prioritization is described in [47].

RUBIES-EGS-QG-1 (R.A. 214.9155459, Dec. 52.9490183) was observed in March 2024 as part of the observations in the EGS field. The MSA pointings were observed for 48 minutes each in the PRISM/CLEAR and the G395M/F290LP spectroscopic modes. Each target was observed in a  $1\times3$  configuration of open microshutters, with a 3-point nodding pattern. The spectra were allowed to overlap on the detector in the G395M exposures as most sources have faint enough continua to not severely contaminate other spectra.

The NIRSpec data are reduced using the msaexp[48] pipeline version 3, the details of which are described in [47]. Briefly, in comparison to version 2 of the pipeline described in [49] we use updated reference files for improved flux calibration. In addition, we leverage empty sky shutters from the RUBIES program to derive custom bar shadow corrections, which we find provide a substantial improvement over the default reference files, removing strong ( $\sim 10\%$  level) unphysical discontinuities in the extracted spectrum. We also use the empty sky shutters to construct a global background subtraction for the PRISM spectra. We use local background subtraction from the nodded exposures for the G395M spectrum, as the overlapping traces on the detector in this mode make it difficult to construct a global background solution. A Gaussian profile is fit to the 2D PRISM spectra to estimate the intrinsic width and centroid of trace. The 1D spectra for both dispersers are then extracted using this Gaussian profile with an optimal weighting [50]. We scale-up the 1- $\sigma$  errors on the 1D extracted spectrum by a factor of 1.7 to account for under-estimated uncertainties when comparing the pixel-to-pixel variations with the msaexp-derived errors [as described in 51]. The final flux calibration of the RUBIES-EGS-QG-1 spectrum is performed by matching the continuum level in the PRISM to the multi-band photometry from HST and JWST/NIRCam, as described in the next Section.

### 2 Photometric data

We use publicly available JWST/NIRCam imaging from the CEERS program [52] as well as program GO-2234 (PI: Bañados; Khusanova et al. in prep.), which combined provide 8 bands of photometry (F090W, F115W, F150W, F200W, F277W, F356W, F444W and F410M).



 $\textbf{Fig. 4} \quad \text{NIRCam F115W and F444W image cutouts of RUBIES-EGS-QG-1}. \ \text{Orange lines show the location of the NIRSpec microshutters}.$ 

We use the reduced image mosaics from the DAWN JWST Archive (DJA; version 7.4). All images were reduced using grizli [53] and have a pixel scale of 0.04 arcsec pix<sup>-1</sup> (see also [10] for further details on the reduction). Next, we use empirical point spread function models (PSF) to construct mosaics that are PSF-matched to the F444W mosaic, as described in [54]. We measure fluxes in circular apertures with a radius of 0.25 arcsec from the PSF-matched photometry, centered on the centroid position estimated by running SourceExtractor[55] on an inverse-variance weighted stack of the F277W, F356W and F444W bands.

We show image cutouts of the F115W and F444W NIRCam filters in Figure 4, and include the position of the NIRSpec microshutters. The centroid of RUBIES-EGS-QG-1 is located in the bottom of the microshutter, with some of the light falling on the bar between two microshutters. Due to the large variation in the PSF width as a function of wavelength, the slit losses introduced by the bar shadow are highly complex, the effect of which we discuss further in Section 3. We also find a faint blue clump in the F115W image, located  $\approx 0.2$  arcsec from RUBIES-EGS-QG-1. In Section 5 we show that emission lines from this source reveal that it is a satellite with a velocity separation of  $\approx 600\,\mathrm{km\,s^{-1}}$ .

## 3 SED modeling

In order to measure the stellar population properties of RUBIES-EGS-QG-1, we utilize the Bayesian SED fitting code Prospector [16, 56, 57] to fit non-parametric star formation histories to the NIRSpec/PRISM spectrum and the JWST/NIRCam photometry of this galaxy. We enforce a signal-to-noise ceiling of 20 on our photometric measurements to account for systematic uncertainties in the underlying stellar population models. We utilize the Flexible Stellar Population Synthesis (FSPS) stellar population synthesis models [58, 59], the MILES spectral library [60], and MIST isochrones [61, 62]. We assume a Chabrier initial mass function [63] and fix the model redshift to  $z_{\rm prism}=4.906$ , the PRISM spectroscopic redshift estimated with msaexp, which differs slightly from the redshift derived from the G395M spectrum due to wavelength calibration uncertainties between the NIRSpec dispersers[64]. We mask the outer edges of the spectrum, to avoid uncertainties in modeling absorption from the

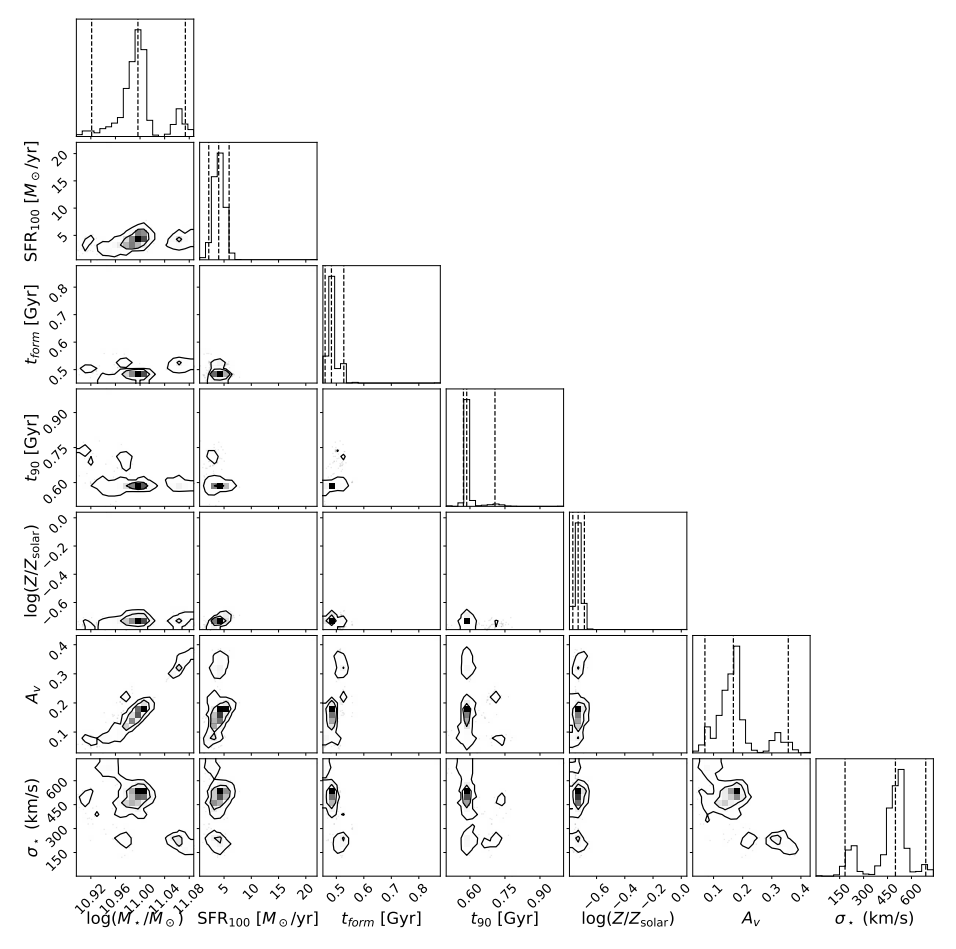


Fig. 5 The covariant posteriors for a selected set of parameters in our fiducial fit with Prospector , with contours bounding 68% and 95% of the likelihood and dashed lines capturing the 95% confidence interval on the marginalized posteriors.

intergalactic medium (i.e. blueward of rest-frame 1200 Å) and the absolute flux calibration at the edge of the NIRSpec CLEAR filter where we do not have photometric coverage (>  $5.1 \,\mu$ m).

Our fiducial star formation history parameterization is a 14-bin non-parametric model utilizing the Prospector continuity prior, with the logarithmic ratio between neighboring bins fit with a Student's t-distribution prior centered 0 with a width of 0.3 and  $\nu=2$  following [65]. We divide the most recent 100 Myr of star formation into three bins of width 5, 25, and 75 Myr respectively to provide fine sampling of the most recent star formation history, and fill the remaining age of the universe with eleven linearly spaced 100 Myr bins. We assume a two-parameter dust law with free  $A_v$  and dust index spanning [0,2.5] and [-1,0.4] respectively [66], and we fix the attenuation around young  $(t < 10^7 \text{ Myr})$  stars to be twice that of the older populations. We fit

for a free logarithmically sampled stellar metallicity in the range of  $[0.1Z_{\odot}, 2Z_{\odot}]$ . We perform sampling using the dynesty nested sampling package [67].

In order to account for the NIRSpec/PRISM resolution, we convolve all models using the JDOX PRISM resolution curve scaled by a multiplicative factor of 1.3 as in [68], which approximates the line spread function of a compact source. As RUBIES-EGS-QG-1 is quite massive, we expect there to be significant intrinsic broadening of the stellar continuum due to the random motions of stars. As such, we fit for an additional free continuum velocity dispersion, with a deliberately large prior  $(\sigma_{\rm smooth} = [0, 1000] \,\rm km \, s^{-1})$  that can also account for uncertainty in the precise normalization of the NIRSpec line spread function. We additionally account for uncertainty in the NIRSpec flux calibration by fitting using the Prospector PolySpecModel prescription, which marginalizes out a 6th order multiplicative polynomial in order to rectify the observed spectrum to the model during each likelihood call. The choice to calibrate out such a high-order polynomial was motivated by the significant wavelength baseline ( $\sim 5 \mu m$ ) of the PRISM spectrum coupled with the considerable uncertainty in the flux calibration on small scales due to the effect of differential slit losses. Because the source is located partially on the bar between two shutters (Figure 4) and the PSF of JWST depends strongly on wavelength, the effect of the bar shadows also has a strong wavelength dependence. Our empirical bar shadow correction (Section 1) derived from blank sky shutters provides only a first order correction of this effect, as the sky emission fills the slit uniformly, but the morphology of RUBIES-EGS-QG-1 follows a steep Sérsic profile (Section 6). This conservative approach utilizes the spectrum only for sharp spectral features such as emission or absorption lines and spectral breaks, and relies on the better-calibrated photometry to fix the shape of the spectral energy distribution. We note that using a lower-order polynomial (e.g. n=1) yields a similarly old, low-metallicity stellar population (also shown in Figure 6), although with a marginally lower stellar mass and more extended star formation history than our fiducial fit. However, we find that this fit has a significantly higher  $\chi^2$  value  $(\chi^2_{n=1} - \chi^2_{n=6} \approx 100)$  and shows oscillatory features in the residuals, indicative of flux calibration issues.

Finally, we account for nebular emission in key emission lines  $(\text{Ly}\alpha_{1216}, [\text{OII}]_{\lambda\lambda3727,3729}, [\text{OIII}]_{\lambda\lambda4960,5008}, \text{H}\delta_{\lambda4103}, \text{H}\gamma_{\lambda4342}, \text{H}\beta_{\lambda4864}, \text{H}\alpha_{\lambda6564}, [\text{NII}]_{\lambda\lambda6549,6585},$ and  $[\text{SII}]_{\lambda\lambda6718,6733})$  using the Prospector nebular marginalization procedure, fitting for emission lines in the residual spectrum using a least squares algorithm and incorporating those models in each likelihood call. This procedure allows the emission lines to be produced without ascribing the emission to a specific source; this is important given the strong evidence for non-star formation sources of ionizing radiation (see Section 5), although our conclusions are unchanged if we do allow for physical nebular infilling of the Balmer absorption lines. Similar to the stellar continuum, we convolve all emission lines with a free emission line velocity dispersion  $\sigma_{\text{gas}} = [0, 1000] \, \text{km s}^{-1}$ , where we assume all emission lines have the same width. In Figure 5, we show the covariant posteriors for key parameters characterizing RUBIES-EGS-QG-1 and demonstrating that the fits are well converged.

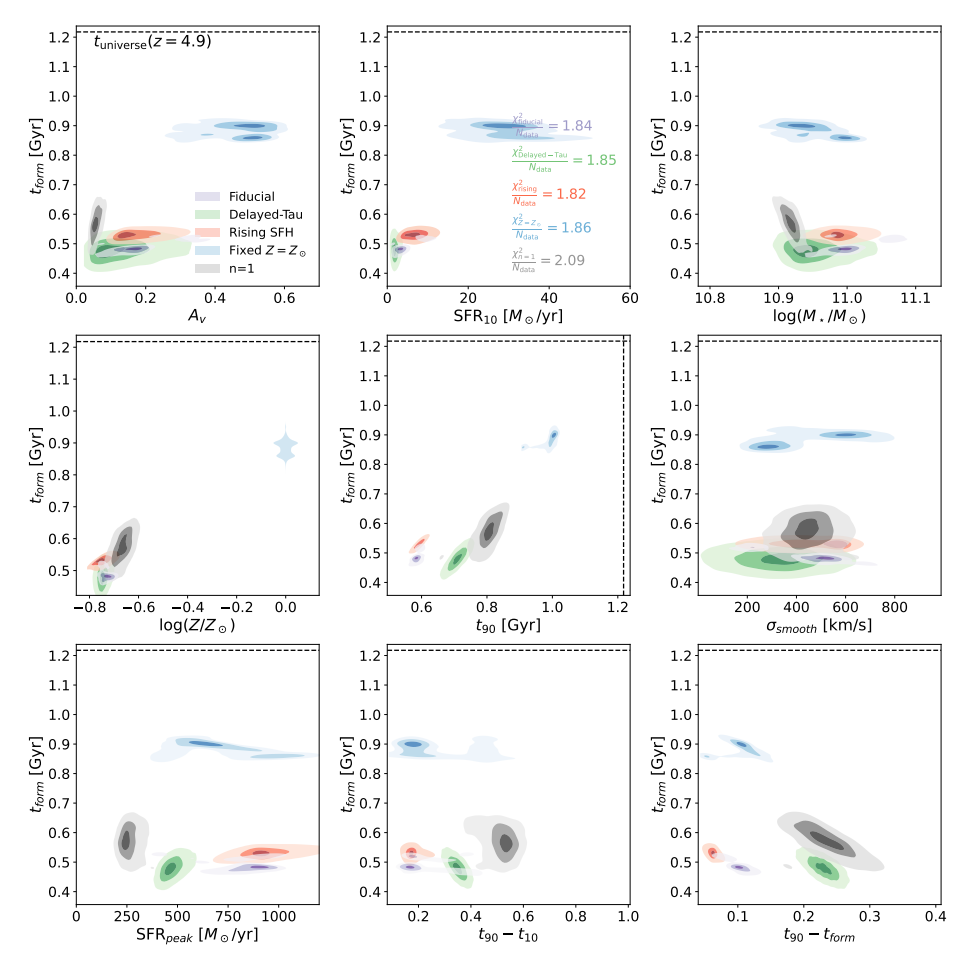


Fig. 6 A comparison of the posteriors of our fiducial (purple), delayed-tau (green), our rising SFH prior (red), fixed  $Z=Z_{\odot}$  (blue), and n=1 polynomial (grey) models, showing the age of the universe when 50% of the galaxy's mass formed,  $t_{\rm form}$ , against the covariant parameters of  $A_V$  (top left), star formation rate (top center), stellar mass (top right), metallicity (middle left),  $t_{90}$ , (the age of the universe when 90% of the galaxy's mass formed, middle center),  $\sigma_{\rm smooth}$  (middle right), SFR<sub>peak</sub> (bottom left), star formation duration timescale ( $t_{90}-t_{10}$ , bottom middle), and star formation decline timescale ( $t_{90}-t_{10}$ , bottom middle), and star formation decline of observation. The fiducial fit, the rising SFH prior fit, and the delayed-tau fits generally agree in reaching old, low-SFR, low-dust, metal-poor solutions. However, fits where we require that the average stellar metallicity to be solar result in a later-forming, more star forming, and dustier galaxy. In the bottom row, we highlight that even when metallicity is fixed to solar, the constraints on the peak star formation rate and the need for a rapid period of intense star formation are consistent with the earlier-forming fiducial model.

## 4 Star formation history testing

The central result of the star formation history fitting of RUBIES-EGS-QG-1 is the finding that the galaxy assembled its high ( $\sim 10^{11} \, \mathrm{M}_{\odot}$ ) stellar mass and ceased forming

stars within only the first billion years of cosmic time, straining galaxy evolution models. Here, we explore how different choices about the parameterization of the star formation history or our priors could impact the inferred age of this system.

First, we examine the impact of choosing a different parameterization of the star formation history. Non-parametric models for the star formation history are commonly chosen because of their flexibility to account for a wide range of star formation history shapes, but such parameterizations systematically measure older ages with increased uncertainty [69]. As a soundness check, we perform our fiducial fit with a star formation history parameterized with the commonly utilized delayed- $\tau$  (SFR  $\propto te^{-t/\tau}$ ) with just three free parameters describing the star formation history, rather than fourteen. We find that this parametric star formation history almost identically recovers that of the non-parametric model, measuring  $t_{\rm form} = 480 \pm ^{30}_{40}$  and recovering similar posteriors for the star formation rate, stellar mass, metallicity, and  $t_{90}$  (see Figure 6 and Table 1), albeit with a slightly longer  $t_{90} - t_{10}$ .

Second, we test our non-parametric star formation history against the choice of prior to mitigate the concern that the inferred star formation history is prior-driven [65, 70]. Instead of the flat prior assumed in our fiducial setup, we impose a rising star formation history prior, as expected from e.g., [71, 72], by shifting the mean logarithmic ratio of our Student's-t prior from 0.0 to 0.3 and re-running our fiducial fit. We find that our measurement of  $t_{\rm form}$  is largely insensitive to the imposition of this prior, and the galaxy is still fit as  $\sim 550$  Myr old, in spite of a slight increase in implied star formation rate and formation time.

We find that both the fiducial fit (insensitive of SFH prior) and delayed-tau fits converge to sub-solar metallicities, with all models suggesting that the metallicity of RUBIES-EGS-QG-1 is 15-20% solar. Our measurements of metallicity are indirect, in the sense that they are sensitive to the shape of the SED rather than specific spectral features, due to the low resolution of the PRISM spectrum and the relative weakness of metal-sensitive features as compared to the bright A-type stars that dominate the light of RUBIES-EGS-QG-1. However, these measurements are qualitatively consistent with the finding that massive quiescent galaxies at z > 1.4 are metal poor relative to solar abundances [17, 73] and with comparably high redshift massive systems [11]. On the other hand, because of a lack of very young metal-poor stars in the Milky Way, empirical model libraries suffer from calibration issues for young ages and low metallicities, which together with uncertainties in the stellar isochrones can have a significant effect on the shape of the continuum of the resulting SPS models [74, 75]. We find that fits utilizing the C3K theoretical stellar libraries [76] rather than the empirical MILES libraries result in low-metallicity solutions within  $\sim 0.1$  dex of our fiducial runs and with comparable age measurements, highlighting that the preference of our fits to these low-metallicity solutions is insensitive to the choice of model libraries. Importantly, however, these model libraries all assume solar abundance patterns. Recent results indicate that deviations in the elemental abundance patterns from the solar abundances used in the SPS models can also lead to incorrectly inferred metallicities [17]. Given that we measure very high  $[N II]/H\alpha$ , which can locally only be

produced in AGN with high metallicity [77], we also fit the galaxy under the assumption of solar metallicity to quantify the effect that a model mismatch would have on the star formation history we infer.

We find that fixing the metallicity to solar has affects the goodness of fit, as evidenced by the slightly worse  $\frac{\chi^2}{N_{\text{data}}}$  values of the fit (see Figure 6). However, this difference is largely driven by differences in the subtle shape of the rest-UV, where the NIRSpec PRISM resolution is worst and where stellar population libraries differ significantly. As such, it is difficult to reject this solution, even if models formally favor low metallicity solutions. The choice to fix the metallicity to solar has a negligible effect on the measured stellar mass, moving the median value by  $\sim 0.05$  dex, but has a considerable impact on the inferred star formation history. At solar metallicity, the observed spectrum and photometry of RUBIES-EGS-QG-1 is best described by a stellar population that formed 50% of its mass ~400 Myr later than the low-metallicity fiducial model. The fit still implies that galaxy assembled the majority of its mass within the first Gyr of cosmic time at the  $2\sigma$  level, but the measured redshift where the galaxy had assembled 90% of its mass (and can be considered to have quenched) shifts from  $8.6\pm^{0.1}_{0.1}$  in the fiducial model to  $5.7\pm^{0.1}_{0.0}$  in the fixed-metallicity model. The fixed-metallicity fit also implies a very similar burst-shape to the fiducial fit; despite the later-formation time, the estimated peak star formation rate, star formation duration, and star formation decline timescale (see the bottom panels in Figure 6) match quite closely between all models. Finally, the fixed-metallicity star formation history still implies an extremely efficient star formation history, requiring  $\epsilon > 0.2$  for the estimated number density of the source (see Figure 2).

Future deep observations that can directly measure metal-sensitive features and that are less beholden to the low resolution of the NIRSpec/PRISM will be able to place more robust constraints on the precise age, metallicity, and dust content of this system. However, despite uncertainty in the exact age of the stellar population, the observed PRISM spectrum and photometry unambiguously demonstrates that RUBIES-EGS-QG-1 is a massive ( $M_* \approx 10^{11} \, \mathrm{M}_{\odot}$ ) quiescent galaxy that assembled the majority of its mass within the first  $\sim 1 \, \mathrm{Gyr}$  of cosmic time before rapidly quenching at z > 5.5, which strains current theoretical models (see Section 8).

### 5 Emission line fitting

The G395M spectrum obtained with JWST/NIRSpec (Figure 7) has a higher spectral resolution ( $R \sim 1000-1500$ ) and resolves the emission line doublets and H $\alpha$  and [N II] complex that are blended in the PRISM spectrum. We also find several emission lines that are spatially offset from the spectrum of RUBIES-EGS-QG-1. Crucially, we find that the lines at 2.95  $\mu$ m and 3.85  $\mu$ m lines are present in both the PRISM and G395M 2D spectra. We identify these lines as [O III] and H $\alpha$  emission from the faint blue source found in the F115W image (Figure 4). Additionally, there is one emission line present in the spectrum at 3.80  $\mu$ m, which is not seen in the PRISM spectrum and implies that it originates from a different source on the NIRSpec MSA: the 2D spectra for the two sources overlap on the detector, because the G395M spectra are longer than the PRISM traces.

Table 1 The resultant median and  $1\sigma$  confidence intervals on a number of key galaxy parameters.

	Fiducial	Delayed-Tau	Rising	$Z=Z_{\odot}$	n=1
$\log(M_{\star}/M_{\odot})$	$11.0\pm^{0.02}_{0.02}$	$10.95\pm_{0.03}^{0.04}$	$10.99\pm_{0.02}^{0.03}$	$10.94\pm_{0.03}^{0.05}$	$10.92\pm^{0.01}_{0.01}$
${ m SFR}_{10}~[M_{\odot}/{ m yr}]$	$3.4\pm^{3.3}_{1.0}$	$2.0\pm^{0.9}_{0.6}$	$7.2\pm^{3.0}_{2.5}$	$28.8\pm^{7.8}_{8.0}$	$0.0\pm^{0.2}_{0.0}$
${ m SFR}_{100}~[M_{\odot}/{ m yr}]$	$4.0\pm^{1.0}_{0.9}$	$2.9\pm^{1.3}_{0.9}$	$7.2\pm^{3.0}_{2.5}$	$27.4\pm^{6.4}_{15.4}$	$0.4\pm^{0.8}_{0.4}$
$\mathrm{SFR}_{peak}~[M_{\odot}/\mathrm{yr}]$	$870\pm_{140}^{70}$	$470\pm_{40}^{60}$	$910\pm_{100}^{140}$	$660\pm^{270}_{160}$	$260\pm_{30}^{60}$
$t_{form}$ [Myr]	$480\pm_{10}^{30}$	$480\pm^{30}_{40}$	$530\pm^{10}_{10}$	$890\pm_{30}^{20}$	$570\pm_{50}^{50}$
$z_{form}$	$10.0\pm^{0.2}_{0.4}$	$9.9\pm^{0.6}_{0.4}$	$9.3\pm^{0.1}_{0.1}$	$6.3\pm_{0.1}^{0.2}$	$8.8\pm^{0.7}_{0.5}$
$t_{90} \; [\mathrm{Myr}]$	$590\pm_{0}^{10}$	$710\pm_{30}^{20}$	$590\pm^{0}_{0}$	$1000\pm^{10}_{30}$	$800\pm^{30}_{30}$
$z_{90}$	$8.6\pm^{0.1}_{0.1}$	$7.4\pm^{0.2}_{0.2}$	$8.5\pm^{0.0}_{0.0}$	$5.7\pm^{0.1}_{0.0}$	$6.8\pm^{0.2}_{0.2}$
$t_{90} - t_{form} \text{ [Myr]}$	$100\pm^{10}_{10}$	$230\pm_{20}^{20}$	$60\pm^{10}_{10}$	$110\pm_{20}^{20}$	$230\pm_{30}^{40}$
$t_{90} - t_{10} \; [\mathrm{Myr}]$	$180\pm_{10}^{170}$	$350\pm^{30}_{30}$	$180\pm_{10}^{20}$	$190\pm^{270}_{10}$	$520\pm^{40}_{70}$
$A_{ m V}  [{ m mag}]$	$0.17\pm_{0.05}^{0.05}$	$0.13\pm^{0.11}_{0.06}$	$0.18\pm^{0.08}_{0.05}$	$0.48\pm_{0.13}^{0.06}$	$0.06\pm^{0.02}_{0.01}$
$\log(Z/Z_{\odot})$	$-0.73\pm^{0.02}_{0.02}$	$-0.75\pm^{0.02}_{0.02}$	$-0.74\pm^{0.02}_{0.02}$	0	$-0.67\pm^{0.04}_{0.04}$

 $<sup>^{1}\</sup>mathrm{SFR}$  averaged over the 10 Myr over observation

We perform a simultaneous fitting to the continuum and [OIII], [NII], [SII] doublets. Although the extraction kernel used to obtain the 1D spectrum mitigates contamination from the satellite and spurious sources, some emission from these sources still appears. We therefore mask the contaminant emission line at  $3.80 \,\mu\text{m}$ , but explicitly include the [O III] and  $H\alpha$  lines of the satellite source in our model. We model each emission line with a Gaussian line profile. The line ratio of [N II] is fixed to 1:2.94, and that of [O III] to 1:2.98. Given the limited signal-to-noise ratio of the emission lines, we assume that all emission (and absorption) lines have the same velocity dispersion, which is a free parameter in the fit. We also include an  $H\alpha$  emission line component, to estimate the infilling of the Balmer absorption line. As the  $H\alpha$  emission may have a different origin from the other emission lines, we leave its velocity dispersion as an additional free parameter. To model the continuum, we use the deconvolved median posterior model from our Prospector fitting to the PRISM spectroscopy. We fit a 1st-order polynomial between this continuum and the G395M spectrum to flux calibrate the spectrum. We assume all components (except for the satellite source) are at the same redshift.

 $<sup>^2{\</sup>rm SFR}$  averaged over the 100 Myr over observation

 $<sup>^3{\</sup>rm The}$  age of the universe when 50% of the galaxy's mass formed

 $<sup>^4</sup>$ The age of the universe when 90% of the galaxy's mass formed

 $<sup>^{5}</sup>A_{
m V}$  surrounding t>10 Myr stars. Our models assume  $A_{
m V}$  is doubled around t<10 Myr stars.

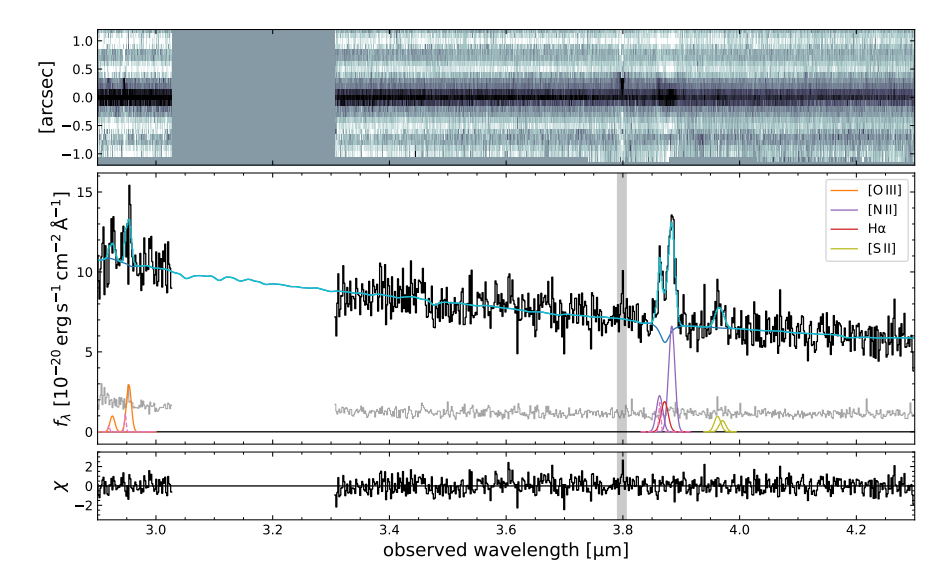


Fig. 7 JWST/NIRSpec medium-resolution spectrum of RUBIES-EGS-QG-1, resolving the [O III], [N II], and [S II] doublets, and the H $\alpha$  line. The 1 $\sigma$  uncertainties are show in gray. The shaded region marks wavelengths that were masked in the fitting, as this emission originates from a source in a different slit in the MSA. The dark blue line shows the median posterior model of the stellar continuum from Prospector. Colored lines show the median posterior models of the emission lines, and the cyan line shows the combined continuum and emission line model. Emission lines originating from a satellite source in the same microshutter, apparent from their spatial offset in the 2D spectrum, are shown with pink dashed lines.

The model is convolved with a custom line spread function (LSF), tailored to the morphology of RUBIES-EGS-QG-1 based on the Sérsic fit at  $4 \,\mu m$ [78]. We allow for uncertainty in the LSF following the method described in [79]. To estimate the posterior distributions of the parameters, we use the emcee package to perform Markov Chain Monte Carlo (MCMC) sampling. We adopt uniform priors for all parameters, allowing for velocity dispersions in the range  $\sigma_{\rm gas} \in [0,750] \, {\rm km \, s^{-1}}$ . We set a broader prior for the H $\alpha$  velocity dispersion,  $\sigma_{\rm H}{\alpha} \in [0,1500] \, {\rm km \, s^{-1}}$ , to test whether there is evidence for a broad line AGN.

The emission line fluxes are reported in Table 2. We show the median posterior model of the combined continuum and emission line fitting in Figure 7, as well as the individual emission line and continuum components. From the fitting we obtain a redshift of  $z_{\rm spec}=4.8976^{+0.0006}_{-0.0010}$  and ionized gas velocity dispersion of  $\sigma_{\rm gas}=414^{+56}_{-64}\,{\rm km\,s^{-1}};$  we find that the velocity dispersion of the H $\alpha$  line converges to a similar value  $\sigma_{\rm H}\alpha=461^{+163}_{-150}\,{\rm km\,s^{-1}}.$  The satellite source has a redshift of  $z_{\rm spec}=4.8885^{+0.0009}_{-0.0009}$  and is thus offset by approximately  $600\,{\rm km\,s^{-1}}$  in the rest frame.

We find very weak H $\alpha$  emission, marginally detected at the  $2\sigma$  level. We hence measure the emission line ratio  $\log([{\rm N\,II}]_{\lambda6585}/{\rm H}\alpha)=0.50^{+0.34}_{-0.25}$ . Although the H $\beta$  line falls outside of the wavelength range covered by the G395M spectrum, we can obtain a lower limit on the H $\beta$  emission line flux by assuming case B recombination (i.e. H $\alpha/{\rm H}\beta=2.86$ ): in this case, the lower limit on the ratio  $\log([{\rm O\,III}]_{\lambda5008}/{\rm H}\beta)=$ 

 $0.50^{+0.31}_{-0.26}$ . These line ratios indicate that the line emission in RUBIES-EGS-QG-1 does not originate from star formation[13]. Although shocked gas also results in high  $[N II]/H\alpha$  line ratios, the ratio inferred from the spectrum and lower limit on the  $[O III]/H\beta$  ratio are most likely consistent with ionization by an AGN[14, 80, 81].

We use the ionized gas velocity dispersion to estimate the dynamical mass using the methodology presented by [82] to relate the gas kinematics to the gravitational potential for compact quiescent galaxies. This assumes the gas forms a rotating disk, with a rotational velocity that is related to the integrated gas velocity dispersion and the inclination (i) of the disk:  $v_{\rm rot} = \sigma_{\rm gas}/(\alpha \sin(i))$ , where  $\alpha \approx 0.8$ . Based on our morphological modeling (Section 6) we find that the projected axis ratio  $q \approx 0.85$ , and assuming an intrinsic disk thickness of  $q_0 = 0.2$  this implies i = 32.5 degrees. The dynamical mass is computed as  $M_{\rm dyn} = 2v_{\rm rot}^2 r_{\rm e}/G$ , where  $r_{\rm e}$  is the inferred half-light radius (Section 6), and G the gravitational constant. With  $r_{\rm e} = 0.55 \pm 0.01$  kpc, we find  $M_{\rm dyn} = 2.7^{+0.7}_{-0.8} \times 10^{11} \,\rm M_{\odot}$ , a factor  $\approx 3$  higher than the measured stellar mass. We note that the gas kinematics may be a biased tracer of the gravitational potential, as the observed stellar and ionized gas kinematics for a large sample of galaxies at  $z \sim 1$  have been shown to agree well on average[83], but with a systematic offset of approximately 0.2 dex for  $\sigma_{\rm gas} \sim 400 \,\rm km \, s^{-1}$ . This may imply that the dynamical mass is overestimated by 0.4 dex (a factor 2.5,  $M_{\rm dyn} \approx 1.1 \times 10^{11} \,\rm M_{\odot}$ ), which is consistent with the estimated stellar mass.

**Table 2** Emission line fluxes of RUBIES-EGS-QG-1 measured from the G395M spectrum.

	flux $[10^{-18}\mathrm{ergs^{-1}cm^{-2}}]$
$\begin{array}{ c c c c c }\hline (O \text{ III}]_{\lambda 4960}\\\hline (O \text{ III}]_{\lambda 5008}\\\hline (N \text{ II}]_{\lambda 6549}\\\hline H\alpha\\\hline (N \text{ II}]_{\lambda 6585}\\\hline (S \text{ II}]_{\lambda 6718}\\\hline (S \text{ II}]_{\lambda 6733}\\\hline \end{array}$	$\begin{array}{c} 1.04 ^{+0.31}_{-0.28} \\ 3.09 ^{+0.92}_{-0.83} \\ 3.09 ^{+0.46}_{-0.51} \\ 2.87 ^{+1.45}_{-1.43} \\ 9.09 ^{+1.36}_{-1.49} \\ 1.36 ^{+0.91}_{-0.55} \\ 0.88 ^{+0.60}_{-0.54} \end{array}$

### 6 Size measurement

We measure the effective radius ( $r_{\rm e}$ ) of RUBIES-EGS-QG-1 as a function of wavelength using the GALFIT [84, 85] single component Sérsic fitting methods from [86] in all available filters (F115W, F150W, F200W, F277W, F356W, F410M, and F444W), corresponding to rest-frame wavelengths in the range  $\sim 2000$  to 7500 Å.

All filters are processed following the procedure described in [87]. Parameters are constrained in the model fits as follows: the magnitude can range  $\pm 3$  mag from the photometric catalog value, radius varies from  $0.01 < r_{\rm e} < 400$  pixels, Sérsic index can range from n = 0.2 to n = 10, and axis ratio from q = 0.0001 (flat) to q = 1 (round).

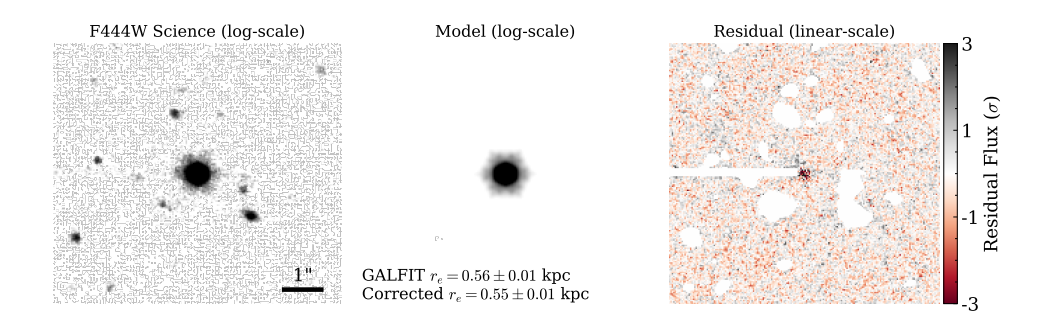


Fig. 8 Sérsic profile fitting for the F444W image reveals a compact light distribution ( $n \approx 9$ ,  $r_e \approx 0.55 \, \mathrm{kpc}$ ).

Next, sizes are corrected to account for residual flux using the methods of [88]. The growth curve from the best-fit Sérsic model (deconvolved from the PSF) is added to the GALFIT residual growth curve. We extrapolate the combined growth curve using the Sérsic model alone when the annular S/N < 3 for the science image. The corrected radius is then defined as the radius where the residual+unconvolved Sérsic growth curve reaches 50%.

We find that RUBIES-EGS-QG-1 is remarkably compact, although we unambiguously resolve this galaxy in F356W, F410M, and F444W. The F444W fit is shown in Figure 8, with a very compact profile ( $n=8.80\pm0.14$ ) and a corrected half-light radius of  $r_{\rm e}=0.55\pm0.01$  kpc (consistent with [89]). The F356W and F410M fits find similar Sérsic index (8.77 and 8.15, respectively) and corrected radii (0.50 and 0.58 kpc), indicating a flat color gradient in the rest-frame optical (3400Å to 7500Å). Given the rapid assembly and quenching of RUBIES-EGS-QG-1 it is not surprising to find a flat color gradient [see, e.g., 90]. The shorter wavelength images (rest-frame < 3000Å) are very compact and have trouble converging to accurate fits without hitting the n=10 upper limit.

### 7 Environment at z = 4.9

Recent studies have speculated on the existence of an overdensity at  $z\approx 5$  in the EGS field, based on a clustering of photometric redshifts[38], and a sample of 4 spectroscopic redshifts at  $z\approx 4.90$  obtained with JWST/NIRSpec[37]. With the addition of RUBIES-EGS-QG-1, this gives a sample of 5 spectroscopic redshifts.

To search for further evidence of a large-scale overdensity, we leverage all available spectroscopic redshifts from JWST/NIRSpec in the EGS field. These spectra come from different JWST Cycle 1 and Cycle 2 programs: the CEERS program, a Director's Discretionary Time program (DDT, #2750; PI Arrabal Haro), and the RUBIES program. All data on the DJA were reduced using the msaexp pipeline[48], in the same manner as described in Section 1. Redshifts were obtained from the spectra using  $\chi^2$  minimization template fitting with msaexp, and visually inspected to evaluate the

quality of the redshifts. The redshifts are predominantly derived from PRISM spectroscopy, although approximately half of the sources in CEERS were observed with the medium-resolution gratings only. We begin by compiling all sources with robust redshifts (grade = 3 from visual inspection) in the range 4 < z < 6 from the DJA, which results in 193 sources from RUBIES, 123 from CEERS and an additional 20 from the DDT program. Of these 336 sources, 289 are detected in NIRCam imaging, with the remainder falling outside of the NIRCam footprint.

We select galaxies within  $\Delta z = \pm 0.0135~(\Delta v = 4000~{\rm km~s^{-1}})$  from the redshift of RUBIES-EGS-QG-1, chosen based on the typical redshift ranges used to search for overdensities (from the compilation in [91]), which is sufficiently large to account for systematic uncertainties in the wavelength calibration of NIRSpec[64]. In total, we find 13 sources in this velocity range around RUBIES-EGS-QG-1 (Figure 9, Table 3), 4 of which were published previously. Of these 13 sources, 6 have a close angular separation to RUBIES-EGS-QG-1 of < 1 arcmin, corresponding to < 400 kpc or < 2 comoving Mpc. We identify another clustering of 4 sources at a distance of  $\approx$  7 arcmin ( $\approx$  16 comoving Mpc) from RUBIES-EGS-QG-1. Interestingly, the brightest source in the F444W imaging among these four (RUBIES-EGS-14295) is a submillimeter galaxy identified from SCUBA-2 850  $\mu$ m data (S2CLS-EGS-850.061; [36]), and implies a high star formation rate. The remaining three sources are scattered across the field at varying distances.

The typical NIRSpec MSA can target approximately  $\sim 200$  sources simultaneously, which generally leads to a complex selection function, in which high-priority targets have a high probability of being allocated a shutter, and any individual galaxy in the broader population has a low probability of being observed [44, 64, 92]. As a result, the spectroscopic completeness is likely to be low at intermediate redshift, as the science objective of the majority of programs focuses on galaxies at z>6. Because of this incompleteness, it is difficult to quantify the overdensity of the spectroscopic targets at the redshift of RUBIES-EGS-QG-1 to estimate its halo mass. However, we can use the 4 < z < 6 galaxy population with robust spectroscopy to assess qualitatively whether RUBIES-EGS-QG-1 is likely to be part of an overdensity. Under the assumption that sources in this redshift range are targeted with approximately equal probability, we can estimate the the typical clustering of galaxies in redshift space and projected distance.

To assess the expected clustering in redshift space, we select the 50 brightest sources in F444W NIRCam imaging among the 336 spectroscopic targets. We then search for sources within a radius of 3 comoving Mpc, approximately 3 times the virial radius of a moderately-sized cluster at z=0 ( $M_{\rm halo}\sim 10^{14.5}\,{\rm M}_{\odot}$ ), and compute the redshift separation between each source and the brightest galaxy. The corresponding distribution in redshift space peaks at  $\Delta z=0$ , but is very broad (Figure 3). Within a range of  $\Delta z=0.027$ , we find that the overdensity around RUBIES-EGS-QG-1 is significantly (3.1 $\sigma$ ) above this background level. If we use a larger aperture, we find only marginal detections of  $2.2\sigma$  (5 Mpc),  $1.5\sigma$  (10 Mpc) and  $1.6\sigma$  (20 Mpc).

Similarly, we select all sources in narrow redshift windows of  $\Delta z = 0.027$ , stepping between z = 4.0 to z = 6.0, and measure the angular separation with respect to the brightest source in the redshift slice. We again find a broad distribution in the projected distance, which we use to estimate the significance of the clustering of sources around

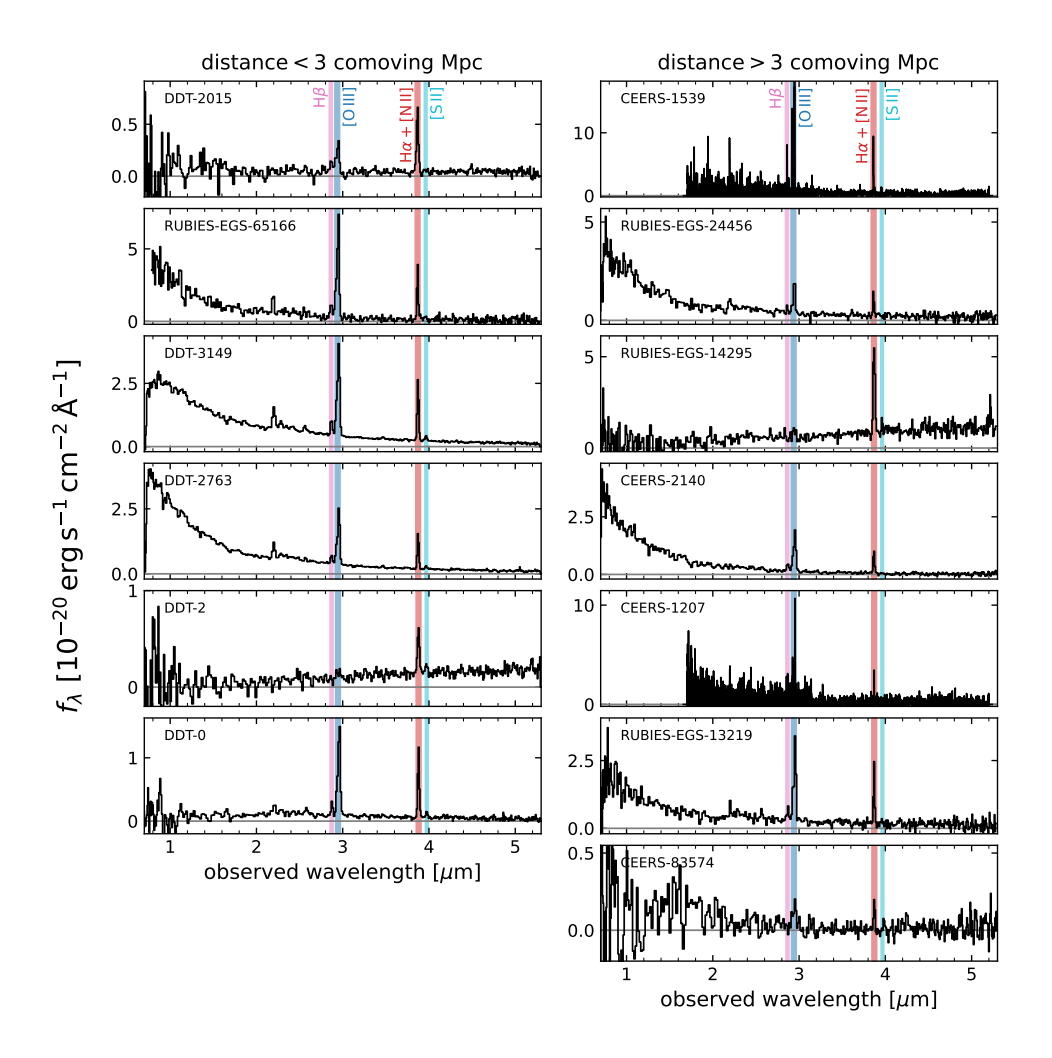


Fig. 9 JWST/NIRSpec spectra of 13 sources with a redshift  $z\approx 4.90$ . The left column shows objects that have a close projected separation to RUBIES-EGS-QG-1, in order of increasing redshift. The right column shows sources in the EGS that are at a larger distance from RUBIES-EGS-QG-1.

RUBIES-EGS-QG-1. Within a radius of 3 Mpc, the neighbors of RUBIES-EGS-QG-1 are  $2.8\sigma$  above the expected level. As before, this decreases when searching within larger apertures:  $2.0\sigma$  within 5 Mpc;  $1.0\sigma$  within 10 Mpc;  $1.44\sigma$  within 20 Mpc.

We conclude that RUBIES-EGS-QG-1 indeed resides in an overdense environment, at least within an aperture of 3 comoving Mpc. Currently this forms the highest redshift overdensity containing a massive quiescent galaxy[39]. However, based on these findings we cannot determine whether RUBIES-EGS-QG-1 resides in a massive halo or in the extremely massive halo needed to reconcile the observed number density of the galaxy with expectations from galaxy formation simulations. Further spectroscopic

follow-up observations will be critical to perform a thorough analysis of the spectroscopic completeness in order to estimate a robust halo mass at the observed redshift, and the projected evolution to the present day.

 $\begin{tabular}{ll} \textbf{Table 3} & Spectroscopically-confirmed sources in the EGS field at the redshift of RUBIES-EGS-QG-1 . \\ \end{tabular}$ 

ID	R.A.	Dec.	z
CEERS-1207 <sup>1</sup>	214.960005	52.831171	4.8957
$CEERS-1539^1$	214.980078	52.942659	4.8840
CEERS- $2140^1$	214.796009	52.715878	4.8927
CEERS-83574	214.949862	52.831306	4.8980
$DDT-0^2$	214.914550	52.943023	4.9098
$DDT-2^{2,3}$	214.909113	52.937204	4.9080
DDT-2015	214.917995	52.937245	4.8903
$DDT-2763^{2}$	214.927789	52.935859	4.9009
$DDT-3149^2$	214.914917	52.943621	4.8991
RUBIES-EGS-13219	214.947589	52.836578	4.8966
RUBIES-EGS-14295	214.943835	52.835816	4.8925
RUBIES-EGS-65166	214.918350	52.931829	4.8919

<sup>&</sup>lt;sup>1</sup>Published in [93].

### 8 Theoretical predictions

We compare the existence and properties of RUBIES-EGS-QG-1 with five different large-volume simulations from recent literature, all of which simulate galaxy formation and evolution within the  $\Lambda$ CDM cosmological model. First, we evaluate the number density of massive quiescent galaxies in the different models:

- The First Light And Reionisation Epoch Simulations (FLARES)[95, 96] uses the EAGLE model[97, 98] to perform hydrodynamical zoom simulations of regions in a volume of 3.2 comoving  ${\rm Gpc}^3$ , thereby probing rare haloes that would not appear in the EAGLE simulation. Using the measurements of [31] based on the combination of FLARES and EAGLE, the predicted surface density of quiescent galaxies at  $z \sim 4.5-5$  and apparent magnitude similar to RUBIES-EGS-QG-1 (F200W < 24.5) is approximately  $0.1-1\,{\rm degree}^{-2}$ , or  $n\sim 1-10\times 10^{-8}\,{\rm Mpc}^{-3}$ .
- In the cosmological hydrodynamical simulation TNG300 of the IllustrisTNG project[99–104], which simulates a comoving volume of  $302\,\mathrm{Mpc^3}$  using the IllustrisTNG model, the population of massive quiescent galaxies has been shown to appear only at  $z\approx 4.2[33]$  in the simulation. At z=5, we find a single system in the simulation that lies within the  $3\sigma$  contours of the stellar mass and SFR of RUBIES-EGS-QG-1 (as measured within an aperture of twice the 3D stellar half-mass radius), corresponding to a comoving number density of  $n=3\times 10^{-8}\,\mathrm{Mpc^{-3}}$ .

<sup>&</sup>lt;sup>2</sup>Published in [37].

 $<sup>^{3}</sup>$ CEERS-DSFG-1 of [94].

- In the cosmological hydrodynamical simulation Magneticum Pathfinder of comoving volume  $180\,\mathrm{Mpc^3}$ , lower-mass quiescent galaxies are present with number densities consistent with observations[32], but no systems were reported at  $M_* \sim 10^{11}\,\mathrm{M_{\odot}}$  at  $z \approx 5$ , setting an upper limit on the number density of  $n < 1 \times 10^{-7}\,\mathrm{Mpc^{-3}}$ .
- The latest version of the semi-analytic GAlaxy Evolution and Assembly (GAEA) model[34, 105–107] was run on the Millennium Simulation[108] of box length 500 Mpc/h (where h=0.73). Within this large volume there are 14 quiescent galaxies of  $\log(M_*/\mathrm{M}_\odot) > 10.9$  at  $z \approx 4.9$ , i.e.  $n=4\times 10^{-8}\,\mathrm{Mpc}^3$ .
- The semi-analytic model SHARKv2.0[35] was run for the SURFS[109] dark matter-only simulation volume of box length 210 Mpc/h (with h=0.6751). Following the methodology of [35], which includes an estimate of the observational uncertainty of 0.25 dex on the inferred number density, the number density of massive  $(\log(M_*/\mathrm{M}_{\odot}) > 10.9)$  quiescent galaxies  $n=2\times10^{-8}\,\mathrm{Mpc}^3$  at z=5.

In summary, we find that the different models all predict the existence of massive quiescent galaxies at high redshifts, but with very low number densities at the redshift of RUBIES-EGS-QG-1, with a typical value of  $n\sim 5\times 10^{-8}\,\mathrm{Mpc^{-3}}$  across the simulations. With an estimated observed number density of  $n\approx 4\times 10^{-6}\,\mathrm{Mpc^{-3}}$ , RUBIES-EGS-QG-1 is therefore an outlier at the  $2\sigma$  level at  $z\approx 5$  if we assume the theoretical model predictions to be accurate. It also implies that, instead of residing in a halo of  $M_{\mathrm{halo}}\sim 10^{12}\,\mathrm{M}_{\odot}$ , the halo mass of RUBIES-EGS-QG-1 would be among the most massive haloes at z=5, as  $M_{\mathrm{halo}}\sim 10^{12.5-13}\,\mathrm{M}_{\odot}$  in the simulations.

However, at higher redshift the tension increases: even for the solar-metallicity model, RUBIES-EGS-QG-1 formed its stars and quenched at  $z \gtrsim 5.5$ . The FLARES simulation predicts an extremely low source density of  $n < 1 \times 10^{-8} \, \mathrm{Mpc^{-3}}$  at  $z \geq 5.5$  (i.e.  $\lesssim 0.1 \, \mathrm{degree^{-2}}$ ), and the GAEA simulations predict similarly low numbers  $(n = 6 \times 10^{-9} \, \mathrm{Mpc^{-3}})$  at  $z \approx 6$ ; both report zero such galaxies at  $z \sim 7$ , which implies that  $n(z = 7) \lesssim 1 \times 10^{-9} \, \mathrm{Mpc^{-3}}$ . The relatively smaller volumes (TNG300, Magneticum Pathfinder) do not appear to contain any quiescent galaxies more massive than  $M_* > 10^{10.9} \, \mathrm{M_{\odot}}$  at  $z \geq 5$ , and do not contain any such massive galaxies at z > 6 even when considering star-forming galaxies. Therefore, if we also account for the unusual formation history of RUBIES-EGS-QG-1, this implies that the probability of finding a source like RUBIES-EGS-QG-1 within the small volume of the NIRCam imaging explored for the RUBIES survey thus far is approximately 0.03% (i.e., an outlier at the  $> 2.8\sigma$  level), and strains current theoretical models.

Lastly, we use the GAEA and TNG300 simulations to explore the possibility that RUBIES-EGS-QG-1 formed through a rapid, major merger of two moderately-massive galaxies. We estimate a merger timescale of  $\sim 200-300\,\mathrm{Myr}[110]$ : because we do not find any signatures of a recent merger in the NIRCam imaging, the merger must have occurred at z>6. We therefore search for the nearest massive neighbor of galaxies of  $\log(M_*/\mathrm{M}_\odot)>10.3$  in the simulations at  $z\gtrsim 6$ . For GAEA, we find two massive pairs that are separated by  $<0.5\,\mathrm{comoving}\,\mathrm{Mpc}$  at z=6.2, and six such pairs at z=5.7, corresponding to a number density of  $6-20\times10^{-9}\,\mathrm{Mpc}^{-3}$ . In TNG300, we find a single pair of massive galaxies at z=6.0, which implies a number density for such equal-mass mergers of  $3\times10^{-8}\,\mathrm{Mpc}^{-3}$ . However, when tracing their merger history, we find that the pair does not merge until z=5.0, which is inconsistent with the lack of merger

signatures in the morphology of RUBIES-EGS-QG-1. These low number densities are therefore upper limits on the expected rate of equal-mass mergers of massive galaxies at high redshift, and indicates that the formation of RUBIES-EGS-QG-1 through such a scenario is expected to be extremely rare.

### 9 NOEMA non-detection

RUBIES-EGS-QG-1 was also covered by NOEMA observations as part of project W20CK (PIs: Buat & Zavala), originally designed to target dusty star-forming galaxy candidates at z>3 (see [94] for further details and the data reduction process). These observations allow us to derive a  $3\sigma$  upper limit at 1.1mm of < 1 mJy. Assuming a typical SED – a modified black-body function with a dust temperature of  $T_{\rm D}=35\,{\rm K}$  and a dust emissivity index of  $\beta=1.8$  – at z=4.9, this flux density upper limit corresponds to an IR luminosity of  $<8\times10^{11}\,L_{\odot}$ . Assuming the calibration between star formation rate and infrared luminosity of [111], this implies a dust-obscured star formation rate of  $<120\,{\rm M}_{\odot}\,{\rm yr}^{-1}$ .

Acknowledgments. We thank V. Buat, D. Burgarella, and J. Zavala for sharing their NOEMA data and constraints on the dust-obscured star formation of RUBIES-EGS-QG-1. This work is partially based on observations carried out under project number W20CK with the IRAM NOEMA Interferometer. IRAM is supported by INSU/CNRS (France), MPG (Germany), and IGN (Spain). We thank Claudia Lagos for providing measurements from the SHARK simulation. This research was supported by the International Space Science Institute (ISSI) in Bern, through ISSI International Team project #562. MVM, JL, and BW acknowledge funding support from NASA via JWST-GO-4233. The Cosmic Dawn Center is funded by the Danish National Research Foundation (DNRF140). This work has received funding from the Swiss State Secretariat for Education, Research and Innovation (SERI) under contract number MB22.00072, as well as from the Swiss National Science Foundation (SNSF) through project grant 200020\_207349. Support for this work was provided by The Brinson Foundation through a Brinson Prize Fellowship grant. Support for this work for RPN was provided by NASA through the NASA Hubble Fellowship grant HST-HF2-51515.001-A awarded by the Space Telescope Science Institute, which is operated by the Association of Universities for Research in Astronomy, Incorporated, under NASA contract NAS5-26555. This work is based on observations made with the NASA/ESA/CSA James Webb Space Telescope. The data were obtained from the Mikulski Archive for Space Telescopes at the Space Telescope Science Institute, which is operated by the Association of Universities for Research in Astronomy, Inc., under NASA contract NAS 5-03127 for JWST. The observations in this work are associated with programs ERS-1345, GO-2234, DDT-2750 and GO-4233. We gratefully acknowledge the CEERS and DDT-2750 teams for developing their observing program with a zero-exclusive-access period.

**Data availability.** The unprocessed JWST data are available through the Mikulski Archive for Space Telescopes. Reduced data from JWST underlying this work are publicly available in the DAWN JWST Archive (https://dawn-cph.github.io/dja/).

Code availability. All software packages used in this work are publicly available on Github: grizli, msafit, msaexp, Prospector, sedpy. The GALFIT software can be found on https://users.obs.carnegiescience.edu/peng/work/galfit/galfit.html.

Author contributions. AdG and GB designed the NIRSpec MSA observations. AdG drafted the main text and led the emission line, environment, and simulation analyses. DJS led the stellar population analysis. GB performed the image and spectroscopic data reduction. SC led the morphological analysis. AW and IL measured the JWST and HST photometry. KAS, JL and MVM contributed to the stellar population analysis. KAS, SP and KEW contributed to the morphological analysis. FV provided the number density estimate. GDL and MH provided measurements from the GAEA simulation. All authors aided in the interpretation of the results and contributed to the Main text and Methods.

**Author Information.** The authors declare that they have no competing financial interests. Correspondence and requests for materials should be addressed to AdG (email: degraaff@mpia.de).

### References

- [1] White, S.D.M., Rees, M.J.: Core condensation in heavy halos: a two-stage theory for galaxy formation and clustering. Mon. Not. R. Astron. Soc. **183**, 341–358 (1978) https://doi.org/10.1093/mnras/183.3.341
- Blumenthal, G.R., Faber, S.M., Primack, J.R., Rees, M.J.: Formation of galaxies and large-scale structure with cold dark matter. Nature 311, 517–525 (1984) https://doi.org/10.1038/311517a0
- [3] Labbé, I., van Dokkum, P., Nelson, E., Bezanson, R., Suess, K.A., Leja, J., Brammer, G., Whitaker, K., Mathews, E., Stefanon, M., Wang, B.: A population of red candidate massive galaxies 600 Myr after the Big Bang. Nature 616(7956), 266–269 (2023) https://doi.org/10.1038/s41586-023-05786-2 arXiv:2207.12446 [astro-ph.GA]
- Boylan-Kolchin, M.: Stress testing ACDM with high-redshift galaxy candidates. Nature Astronomy 7, 731–735 (2023) https://doi.org/10.1038/s41550-023-01937-7 arXiv:2208.01611 [astro-ph.CO]
- [5] Behroozi, P., Silk, J.: The most massive galaxies and black holes allowed by ΛCDM. Mon. Not. R. Astron. Soc. 477(4), 5382–5387 (2018) https://doi.org/ 10.1093/mnras/sty945 arXiv:1609.04402 [astro-ph.GA]
- [6] Xiao, M., Oesch, P., Elbaz, D., Bing, L., Nelson, E., Weibel, A., Naidu, R., Daddi, E., Bouwens, R., Matthee, J., Wuyts, S., Chisholm, J., Brammer, G., Dickinson, M., Magnelli, B., Leroy, L., van Dokkum, P., Schaerer, D., Herard-Demanche, T., Barrufet, L., Endsley, R., Fudamoto, Y., Gómez-Guijarro, C., Gottumukkala, R., Illingworth, G., Labbe, I., Magee, D., Marchesini, D., Maseda, M., Qin, Y.,

- Reddy, N., Shapley, A., Shivaei, I., Shuntov, M., Stefanon, M., Whitaker, K., Wyithe, J.S.: Massive Optically Dark Galaxies Unveiled by JWST Challenge Galaxy Formation Models. arXiv e-prints, 2309–02492 (2023) https://doi.org/10.48550/arXiv.2309.02492 arXiv.2309.02492 [astro-ph.GA]
- [7] Glazebrook, K., Schreiber, C., Labbé, I., Nanayakkara, T., Kacprzak, G.G., Oesch, P.A., Papovich, C., Spitler, L.R., Straatman, C.M.S., Tran, K.-V.H., Yuan, T.: A massive, quiescent galaxy at a redshift of 3.717. Nature 544(7648), 71–74 (2017) https://doi.org/10.1038/nature21680 arXiv:1702.01751 [astro-ph.GA]
- [8] Valentino, F., Tanaka, M., Davidzon, I., Toft, S., Gómez-Guijarro, C., Stockmann, M., Onodera, M., Brammer, G., Ceverino, D., Faisst, A.L., Gallazzi, A., Hayward, C.C., Ilbert, O., Kubo, M., Magdis, G.E., Selsing, J., Shimakawa, R., Sparre, M., Steinhardt, C., Yabe, K., Zabl, J.: Quiescent Galaxies 1.5 Billion Years after the Big Bang and Their Progenitors. Astrophys. J. 889(2), 93 (2020) https://doi.org/10.3847/1538-4357/ab64dc arXiv:1909.10540 [astro-ph.GA]
- [9] Carnall, A.C., McLure, R.J., Dunlop, J.S., McLeod, D.J., Wild, V., Cullen, F., Magee, D., Begley, R., Cimatti, A., Donnan, C.T., Hamadouche, M.L., Jewell, S.M., Walker, S.: A massive quiescent galaxy at redshift 4.658. Nature 619(7971), 716–719 (2023) https://doi.org/10.1038/s41586-023-06158-6 arXiv:2301.11413 [astro-ph.GA]
- [10] Valentino, F., Brammer, G., Gould, K.M.L., Kokorev, V., Fujimoto, S., Jespersen, C.K., Vijayan, A.P., Weaver, J.R., Ito, K., Tanaka, M., Ilbert, O., Magdis, G.E., Whitaker, K.E., Faisst, A.L., Gallazzi, A., Gillman, S., Giménez-Arteaga, C., Gómez-Guijarro, C., Kubo, M., Heintz, K.E., Hirschmann, M., Oesch, P., Onodera, M., Rizzo, F., Lee, M., Strait, V., Toft, S.: An Atlas of Color-selected Quiescent Galaxies at z ¿ 3 in Public JWST Fields. Astrophys. J. 947(1), 20 (2023) https://doi.org/10.3847/1538-4357/acbefa arXiv:2302.10936 [astro-ph.GA]
- [11] Carnall, A.C., McLeod, D.J., McLure, R.J., Dunlop, J.S., Begley, R., Cullen, F., Donnan, C.T., Hamadouche, M.L., Jewell, S.M., Jones, E.W., Pollock, C.L., Wild, V.: A surprising abundance of massive quiescent galaxies at 3 ; z ; 5 in the first data from JWST CEERS. Mon. Not. R. Astron. Soc. 520(3), 3974–3985 (2023) https://doi.org/10.1093/mnras/stad369 arXiv:2208.00986 [astro-ph.GA]
- [12] Urbano Stawinski, S.M., Cooper, M.C., Forrest, B., Muzzin, A., Marchesini, D., Wilson, G., Gomez, P., McConachie, I., Marsan, Z.C., Annuziatella, M., Chang, W.: Spectroscopic Confirmation of an Ultra-Massive Galaxy in a Protocluster at  $z\sim4.9$ . The Open Journal of Astrophysics 7, 46 (2024) https://doi.org/10.33232/001c.120087 arXiv:2404.16036 [astro-ph.GA]
- [13] Kewley, L.J., Dopita, M.A., Sutherland, R.S., Heisler, C.A., Trevena, J.: Theoretical Modeling of Starburst Galaxies. Astrophys. J. **556**(1), 121–140 (2001)

- [14] Kewley, L.J., Groves, B., Kauffmann, G., Heckman, T.: The host galaxies and classification of active galactic nuclei. Mon. Not. R. Astron. Soc. 372(3), 961–976 (2006) https://doi.org/10.1111/j.1365-2966.2006.10859.x arXiv:astroph/0605681 [astro-ph]
- [15] Goto, T.: A catalogue of local E+A (post-starburst) galaxies selected from the Sloan Digital Sky Survey Data Release 5. Mon. Not. R. Astron. Soc. 381(1), 187– 193 (2007) https://doi.org/10.1111/j.1365-2966.2007.12227.x arXiv:0801.1106 [astro-ph]
- [16] Johnson, B., Foreman-Mackey, D., Sick, J., Leja, J., Byler, N., Walmsley, M., Tollerud, E., Leung, H., Scott, S.: dfm/python-fsps: python-fsps v0.4.0. Zenodo (2021). https://doi.org/10.5281/zenodo.4577191
- [17] Beverage, A.G., Slob, M., Kriek, M., Conroy, C., Barro, G., Bezanson, R., Brammer, G., Cheng, C.M., de Graaff, A., Förster Schreiber, N.M., Franx, M., Lorenz, B., Mancera Piña, P.E., Marchesini, D., Muzzin, A., Newman, A.B., Price, S.H., Shapley, A.E., Stefanon, M., Suess, K.A., van Dokkum, P., Weinberg, D., Weisz, D.R.: Carbon and Iron Deficiencies in Quiescent Galaxies at z=1-3 from JWST-SUSPENSE: Implications for the Formation Histories of Massive Galaxies. arXiv e-prints, 2407–02556 (2024) https://doi.org/10.48550/arXiv.2407.02556 arXiv:2407.02556 [astro-ph.GA]
- [18] de Graaff, A., Pillepich, A., Rix, H.-W.: An early dark matter-dominated phase in the assembly history of Milky Way-mass galaxies suggested by the TNG50 simulation and JWST observations. arXiv e-prints, 2403–00907 (2024) https: //doi.org/10.48550/arXiv.2403.00907 arXiv:2403.00907 [astro-ph.GA]
- [19] Hopkins, P.F., Murray, N., Quataert, E., Thompson, T.A.: A maximum stellar surface density in dense stellar systems. Mon. Not. R. Astron. Soc. 401(1), 19–23 (2010) https://doi.org/10.1111/j.1745-3933.2009.00777.x arXiv:0908.4088 [astro-ph.CO]
- [20] Grudić, M.Y., Hopkins, P.F., Quataert, E., Murray, N.: The maximum stellar surface density due to the failure of stellar feedback. Mon. Not. R. Astron. Soc. **483**(4), 5548–5553 (2019) https://doi.org/10.1093/mnras/sty3386 arXiv:1804.04137 [astro-ph.GA]
- [21] Franx, M., van Dokkum, P.G., Förster Schreiber, N.M., Wuyts, S., Labbé, I., Toft, S.: Structure and Star Formation in Galaxies out to z = 3: Evidence for Surface Density Dependent Evolution and Upsizing. Astrophys. J. 688(2), 770– 788 (2008) https://doi.org/10.1086/592431 arXiv:0808.2642 [astro-ph]
- [22] Whitaker, K.E., Bezanson, R., van Dokkum, P.G., Franx, M., van der Wel, A., Brammer, G., Förster-Schreiber, N.M., Giavalisco, M., Labbé, I., Momcheva,

- I.G., Nelson, E.J., Skelton, R.: Predicting Quiescence: The Dependence of Specific Star Formation Rate on Galaxy Size and Central Density at 0.5 ; z ; 2.5. Astrophys. J. 838(1), 19 (2017) https://doi.org/10.3847/1538-4357/aa6258 arXiv:1607.03107 [astro-ph.GA]
- [23] Barro, G., Faber, S.M., Pérez-González, P.G., Koo, D.C., Williams, C.C., Kocevski, D.D., Trump, J.R., Mozena, M., McGrath, E., van der Wel, A., Wuyts, S., Bell, E.F., Croton, D.J., Ceverino, D., Dekel, A., Ashby, M.L.N., Cheung, E., Ferguson, H.C., Fontana, A., Fang, J., Giavalisco, M., Grogin, N.A., Guo, Y., Hathi, N.P., Hopkins, P.F., Huang, K.-H., Koekemoer, A.M., Kartaltepe, J.S., Lee, K.-S., Newman, J.A., Porter, L.A., Primack, J.R., Ryan, R.E., Rosario, D., Somerville, R.S., Salvato, M., Hsu, L.-T.: CANDELS: The Progenitors of Compact Quiescent Galaxies at z ~2. Astrophys. J. 765(2), 104 (2013) https://doi.org/10.1088/0004-637X/765/2/104 arXiv:1206.5000 [astro-ph.CO]
- [24] Bouwens, R.J., Smit, R., Schouws, S., Stefanon, M., Bowler, R., Endsley, R., Gonzalez, V., Inami, H., Stark, D., Oesch, P., Hodge, J., Aravena, M., da Cunha, E., Dayal, P., de Looze, I., Ferrara, A., Fudamoto, Y., Graziani, L., Li, C., Nanayakkara, T., Pallottini, A., Schneider, R., Sommovigo, L., Topping, M., van der Werf, P., Algera, H., Barrufet, L., Hygate, A., Labbé, I., Riechers, D., Witstok, J.: Reionization Era Bright Emission Line Survey: Selection and Characterization of Luminous Interstellar Medium Reservoirs in the z ¿ 6.5 Universe. Astrophys. J. 931(2), 160 (2022) https://doi.org/10.3847/1538-4357/ac5a4a arXiv:2106.13719 [astro-ph.GA]
- [25] Zavala, J.A., Montaña, A., Hughes, D.H., Yun, M.S., Ivison, R.J., Valiante, E., Wilner, D., Spilker, J., Aretxaga, I., Eales, S., Avila-Reese, V., Chávez, M., Cooray, A., Dannerbauer, H., Dunlop, J.S., Dunne, L., Gómez-Ruiz, A.I., Michałowski, M.J., Narayanan, G., Nayyeri, H., Oteo, I., Rosa González, D., Sánchez-Argüelles, D., Schloerb, F.P., Serjeant, S., Smith, M.W.L., Terlevich, E., Vega, O., Villalba, A., van der Werf, P., Wilson, G.W., Zeballos, M.: A dusty star-forming galaxy at z = 6 revealed by strong gravitational lensing. Nature Astronomy 2, 56–62 (2018) https://doi.org/10.1038/s41550-017-0297-8 arXiv:1707.09022 [astro-ph.GA]
- [26] Strandet, M.L., Weiss, A., De Breuck, C., Marrone, D.P., Vieira, J.D., Aravena, M., Ashby, M.L.N., Béthermin, M., Bothwell, M.S., Bradford, C.M., Carlstrom, J.E., Chapman, S.C., Cunningham, D.J.M., Chen, C.-C., Fassnacht, C.D., Gonzalez, A.H., Greve, T.R., Gullberg, B., Hayward, C.C., Hezaveh, Y., Litke, K., Ma, J., Malkan, M., Menten, K.M., Miller, T., Murphy, E.J., Narayanan, D., Phadke, K.A., Rotermund, K.M., Spilker, J.S., Sreevani, J.: ISM Properties of a Massive Dusty Star-forming Galaxy Discovered at z ~ 7. Astrophys. J. Lett. 842(2), 15 (2017) https://doi.org/10.3847/2041-8213/aa74b0 arXiv:1705.07912 [astro-ph.GA]
- [27] Wang, B., Leja, J., de Graaff, A., Brammer, G.B., Weibel, A., van Dokkum,

- P., Baggen, J.F.W., Suess, K.A., Greene, J.E., Bezanson, R., Cleri, N.J., Hirschmann, M., Labbé, I., Matthee, J., McConachie, I., Naidu, R.P., Nelson, E., Oesch, P.A., Setton, D.J., Williams, C.C.: RUBIES: Evolved Stellar Populations with Extended Formation Histories at z  $\sim$  7–8 in Candidate Massive Galaxies Identified with JWST/NIRSpec. Astrophys. J. Lett.  $\bf 969(1)$ , 13 (2024) https://doi.org/10.3847/2041-8213/ad55f7 arXiv:2405.01473 [astro-ph.GA]
- [28] Schouws, S., Stefanon, M., Bouwens, R., Smit, R., Hodge, J., Labbé, I., Algera, H., Boogaard, L., Carniani, S., Fudamoto, Y., Holwerda, B.W., Illingworth, G.D., Maiolino, R., Maseda, M., Oesch, P., van der Werf, P.: Significant Dust-obscured Star Formation in Luminous Lyman-break Galaxies at z 7-8. Astrophys. J. 928(1), 31 (2022) https://doi.org/10.3847/1538-4357/ac4605 arXiv:2105.12133 [astro-ph.GA]
- [29] Wechsler, R.H., Tinker, J.L.: The Connection Between Galaxies and Their Dark Matter Halos. Annu. Rev. Astron. Astrophys. 56, 435–487 (2018) https://doi. org/10.1146/annurev-astro-081817-051756 arXiv:1804.03097 [astro-ph.GA]
- [30] Planck Collaboration, Aghanim, N., Akrami, Y., Ashdown, M., Aumont, J., Baccigalupi, C., Ballardini, M., Banday, A.J., Barreiro, R.B., Bartolo, N., Basak, S., Battye, R., Benabed, K., Bernard, J.-P., Bersanelli, M., Bielewicz, P., Bock, J.J., Bond, J.R., Borrill, J., Bouchet, F.R., Boulanger, F., Bucher, M., Burigana, C., Butler, R.C., Calabrese, E., Cardoso, J.-F., Carron, J., Challinor, A., Chiang, H.C., Chluba, J., Colombo, L.P.L., Combet, C., Contreras, D., Crill, B.P., Cuttaia, F., de Bernardis, P., de Zotti, G., Delabrouille, J., Delouis, J.-M., Di Valentino, E., Diego, J.M., Doré, O., Douspis, M., Ducout, A., Dupac, X., Dusini, S., Efstathiou, G., Elsner, F., Enßlin, T.A., Eriksen, H.K., Fantaye, Y., Farhang, M., Fergusson, J., Fernandez-Cobos, R., Finelli, F., Forastieri, F., Frailis, M., Fraisse, A.A., Franceschi, E., Frolov, A., Galeotta, S., Galli, S., Ganga, K., Génova-Santos, R.T., Gerbino, M., Ghosh, T., González-Nuevo, J., Górski, K.M., Gratton, S., Gruppuso, A., Gudmundsson, J.E., Hamann, J., Handley, W., Hansen, F.K., Herranz, D., Hildebrandt, S.R., Hivon, E., Huang, Z., Jaffe, A.H., Jones, W.C., Karakci, A., Keihänen, E., Keskitalo, R., Kiiveri, K., Kim, J., Kisner, T.S., Knox, L., Krachmalnicoff, N., Kunz, M., Kurki-Suonio, H., Lagache, G., Lamarre, J.-M., Lasenby, A., Lattanzi, M., Lawrence, C.R., Le Jeune, M., Lemos, P., Lesgourgues, J., Levrier, F., Lewis, A., Liguori, M., Lilje, P.B., Lilley, M., Lindholm, V., López-Caniego, M., Lubin, P.M., Ma, Y.-Z., Macías-Pérez, J.F., Maggio, G., Maino, D., Mandolesi, N., Mangilli, A., Marcos-Caballero, A., Maris, M., Martin, P.G., Martinelli, M., Martínez-González, E., Matarrese, S., Mauri, N., McEwen, J.D., Meinhold, P.R., Melchiorri, A., Mennella, A., Migliaccio, M., Millea, M., Mitra, S., Miville-Deschênes, M.-A., Molinari, D., Montier, L., Morgante, G., Moss, A., Natoli, P., Nørgaard-Nielsen, H.U., Pagano, L., Paoletti, D., Partridge, B., Patanchon, G., Peiris, H.V., Perrotta, F., Pettorino, V., Piacentini, F., Polastri, L., Polenta, G., Puget, J.-L., Rachen, J.P., Reinecke, M., Remazeilles, M., Renzi, A., Rocha, G., Rosset, C., Roudier, G., Rubiño-Martín, J.A., Ruiz-Granados, B., Salvati,

- L., Sandri, M., Savelainen, M., Scott, D., Shellard, E.P.S., Sirignano, C., Sirri, G., Spencer, L.D., Sunyaev, R., Suur-Uski, A.-S., Tauber, J.A., Tavagnacco, D., Tenti, M., Toffolatti, L., Tomasi, M., Trombetti, T., Valenziano, L., Valiviita, J., Van Tent, B., Vibert, L., Vielva, P., Villa, F., Vittorio, N., Wandelt, B.D., Wehus, I.K., White, M., White, S.D.M., Zacchei, A., Zonca, A.: Planck 2018 results. VI. Cosmological parameters. Astron. Astrophys. **641**, 6 (2020) https://doi.org/10.1051/0004-6361/201833910 arXiv:1807.06209 [astro-ph.CO]
- [31] Lovell, C.C., Roper, W., Vijayan, A.P., Seeyave, L., Irodotou, D., Wilkins, S.M., Conselice, C.J., Fortuni, F., Kuusisto, J.K., Merlin, E., Santini, P., Thomas, P.: First light and reionisation epoch simulations (FLARES) VIII. The emergence of passive galaxies at  $z \geq 5$ . Mon. Not. R. Astron. Soc. 525(4), 5520-5539 (2023) https://doi.org/10.1093/mnras/stad2550 arXiv:2211.07540 [astro-ph.GA]
- [32] Kimmig, L.C., Remus, R.-S., Seidel, B., Valenzuela, L.M., Dolag, K., Burkert, A.: Blowing out the Candle: How to Quench Galaxies at High Redshift an Ensemble of Rapid Starbursts, AGN Feedback and Environment. arXiv e-prints, 2310–16085 (2023) https://doi.org/10.48550/arXiv.2310.16085 arXiv:2310.16085 [astro-ph.GA]
- [33] Hartley, A.I., Nelson, E.J., Suess, K.A., Garcia, A.M., Park, M., Hernquist, L., Bezanson, R., Nevin, R., Pillepich, A., Schechter, A.L., Terrazas, B.A., Torrey, P., Wellons, S., Whitaker, K.E., Williams, C.C.: The first quiescent galaxies in TNG300. Mon. Not. R. Astron. Soc. 522(2), 3138–3144 (2023) https://doi.org/10.1093/mnras/stad1162 arXiv:2304.09392 [astro-ph.GA]
- [34] De Lucia, G., Fontanot, F., Xie, L., Hirschmann, M.: Tracing the Quenching Journey across Cosmic Time. arXiv e-prints, 2401–06211 (2024) https://doi.org/ 10.48550/arXiv.2401.06211 arXiv:2401.06211 [astro-ph.GA]
- [35] Lagos, C.d.P., Bravo, M., Tobar, R., Obreschkow, D., Power, C., Robotham, A.S.G., Proctor, K.L., Hansen, S., Chandro-Gómez, Á., Carrivick, J.: Quenching massive galaxies across cosmic time with the semi-analytic model SHARK V2.0. Mon. Not. R. Astron. Soc. 531(3), 3551–3578 (2024) https://doi.org/10.1093/mnras/stae1024 arXiv:2309.02310 [astro-ph.GA]
- [36] Zavala, J.A., Aretxaga, I., Geach, J.E., Hughes, D.H., Birkinshaw, M., Chapin, E., Chapman, S., Chen, C.-C., Clements, D.L., Dunlop, J.S., Farrah, D., Ivison, R.J., Jenness, T., Michałowski, M.J., Robson, E.I., Scott, D., Simpson, J., Spaans, M., van der Werf, P.: The SCUBA-2 Cosmology Legacy Survey: the EGS deep field I. Deep number counts and the redshift distribution of the recovered cosmic infrared background at 450 and 850 μ m. Mon. Not. R. Astron. Soc. 464(3), 3369–3384 (2017) https://doi.org/10.1093/mnras/stw2630 arXiv:1610.03551 [astro-ph.GA]
- [37] Arrabal Haro, P., Dickinson, M., Finkelstein, S.L., Kartaltepe, J.S., Donnan,

- C.T., Burgarella, D., Carnall, A.C., Cullen, F., Dunlop, J.S., Fernández, V., Fujimoto, S., Jung, I., Krips, M., Larson, R.L., Papovich, C., Pérez-González, P.G., Amorín, R.O., Bagley, M.B., Buat, V., Casey, C.M., Chworowsky, K., Cohen, S.H., Ferguson, H.C., Giavalisco, M., Huertas-Company, M., Hutchison, T.A., Kocevski, D.D., Koekemoer, A.M., Lucas, R.A., McLeod, D.J., McLure, R.J., Pirzkal, N., Seillé, L.-M., Trump, J.R., Weiner, B.J., Wilkins, S.M., Zavala, J.A.: Confirmation and refutation of very luminous galaxies in the early Universe. Nature 622(7984), 707–711 (2023) https://doi.org/10.1038/s41586-023-06521-7arXiv:2303.15431 [astro-ph.GA]
- [38] Naidu, R.P., Oesch, P.A., Setton, D.J., Matthee, J., Conroy, C., Johnson, B.D., Weaver, J.R., Bouwens, R.J., Brammer, G.B., Dayal, P., Illingworth, G.D., Barrufet, L., Belli, S., Bezanson, R., Bose, S., Heintz, K.E., Leja, J., Leonova, E., Marques-Chaves, R., Stefanon, M., Toft, S., van der Wel, A., van Dokkum, P., Weibel, A., Whitaker, K.E.: Schrodinger's Galaxy Candidate: Puzzlingly Luminous at  $z\approx 17$ , or Dusty/Quenched at  $z\approx 5$ ? arXiv e-prints, 2208–02794 (2022) https://doi.org/10.48550/arXiv.2208.02794 arXiv:2208.02794 [astro-ph.GA]
- [39] Kakimoto, T., Tanaka, M., Onodera, M., Shimakawa, R., Wu, P.-F., Gould, K.M.L., Ito, K., Jin, S., Kubo, M., Suzuki, T.L., Toft, S., Valentino, F., Yabe, K.: A Massive Quiescent Galaxy in a Group Environment at z = 4.53. Astrophys. J. 963(1), 49 (2024) https://doi.org/10.3847/1538-4357/ad1ff1 arXiv:2308.15011 [astro-ph.GA]
- [40] Di Matteo, T., Springel, V., Hernquist, L.: Energy input from quasars regulates the growth and activity of black holes and their host galaxies. Nature 433(7026), 604–607 (2005) https://doi.org/10.1038/nature03335 arXiv:astro-ph/0502199 [astro-ph]
- [41] Nanayakkara, T., Glazebrook, K., Jacobs, C., Kawinwanichakij, L., Schreiber, C., Brammer, G., Esdaile, J., Kacprzak, G.G., Labbe, I., Lagos, C., Marchesini, D., Marsan, Z.C., Oesch, P.A., Papovich, C., Remus, R.-S., Tran, K.-V.H.: A population of faint, old, and massive quiescent galaxies at 3 jz j4 revealed by JWST NIRSpec Spectroscopy. Scientific Reports 14, 3724 (2024) https://doi.org/10.1038/s41598-024-52585-4 arXiv:2212.11638 [astro-ph.GA]
- [42] Glazebrook, K., Nanayakkara, T., Schreiber, C., Lagos, C., Kawinwanichakij, L., Jacobs, C., Chittenden, H., Brammer, G., Kacprzak, G.G., Labbe, I., Marchesini, D., Marsan, Z.C., Oesch, P.A., Papovich, C., Remus, R.-S., Tran, K.-V.H., Esdaile, J., Chandro Gomez, A.: A massive galaxy that formed its stars at  $z\sim11$ . arXiv e-prints, 2308–05606 (2023) https://doi.org/10.48550/arXiv.2308.05606 arXiv:2308.05606 [astro-ph.GA]
- [43] Antwi-Danso, J., Papovich, C., Esdaile, J., Nanayakkara, T., Glazebrook, K., Hutchison, T.A., Whitaker, K.E., Marsan, Z.C., Diaz, R.J., Marchesini, D., Muzzin, A., Tran, K.-V.H., Setton, D.J., Kaushal, Y., Speagle, J.S., Cole, J.:

- The FENIKS Survey: Spectroscopic Confirmation of Massive Quiescent Galaxies at z ~3-5. arXiv e-prints, 2307–09590 (2023) https://doi.org/10.48550/arXiv.2307.09590 arXiv:2307.09590 [astro-ph.GA]
- [44] Ferruit, P., Jakobsen, P., Giardino, G., Rawle, T., Alves de Oliveira, C., Arribas, S., Beck, T.L., Birkmann, S., Böker, T., Bunker, A.J., Charlot, S., de Marchi, G., Franx, M., Henry, A., Karakla, D., Kassin, S.A., Kumari, N., López-Caniego, M., Lützgendorf, N., Maiolino, R., Manjavacas, E., Marston, A., Moseley, S.H., Muzerolle, J., Pirzkal, N., Rauscher, B., Rix, H.-W., Sabbi, E., Sirianni, M., te Plate, M., Valenti, J., Willott, C.J., Zeidler, P.: The Near-Infrared Spectrograph (NIRSpec) on the James Webb Space Telescope. II. Multi-object spectroscopy (MOS). Astron. Astrophys. 661, 81 (2022) https://doi.org/10.1051/0004-6361/202142673 arXiv:2202.03306 [astro-ph.IM]
- [45] Koekemoer, A.M., Faber, S.M., Ferguson, H.C., Grogin, N.A., Kocevski, D.D., Koo, D.C., Lai, K., Lotz, J.M., Lucas, R.A., McGrath, E.J., Ogaz, S., Rajan, A., Riess, A.G., Rodney, S.A., Strolger, L., Casertano, S., Castellano, M., Dahlen, T., Dickinson, M., Dolch, T., Fontana, A., Giavalisco, M., Grazian, A., Guo, Y., Hathi, N.P., Huang, K.-H., van der Wel, A., Yan, H.-J., Acquaviva, V., Alexander, D.M., Almaini, O., Ashby, M.L.N., Barden, M., Bell, E.F., Bournaud, F., Brown, T.M., Caputi, K.I., Cassata, P., Challis, P.J., Chary, R.-R., Cheung, E., Cirasuolo, M., Conselice, C.J., Roshan Cooray, A., Croton, D.J., Daddi, E., Davé, R., de Mello, D.F., de Ravel, L., Dekel, A., Donley, J.L., Dunlop, J.S., Dutton, A.A., Elbaz, D., Fazio, G.G., Filippenko, A.V., Finkelstein, S.L., Frazer, C., Gardner, J.P., Garnavich, P.M., Gawiser, E., Gruetzbauch, R., Hartley, W.G., Häussler, B., Herrington, J., Hopkins, P.F., Huang, J.-S., Jha, S.W., Johnson, A., Kartaltepe, J.S., Khostovan, A.A., Kirshner, R.P., Lani, C., Lee, K.-S., Li, W., Madau, P., McCarthy, P.J., McIntosh, D.H., McLure, R.J., McPartland, C., Mobasher, B., Moreira, H., Mortlock, A., Moustakas, L.A., Mozena, M., Nandra, K., Newman, J.A., Nielsen, J.L., Niemi, S., Noeske, K.G., Papovich, C.J., Pentericci, L., Pope, A., Primack, J.R., Ravindranath, S., Reddy, N.A., Renzini, A., Rix, H.-W., Robaina, A.R., Rosario, D.J., Rosati, P., Salimbeni, S., Scarlata, C., Siana, B., Simard, L., Smidt, J., Snyder, D., Somerville, R.S., Spinrad, H., Straughn, A.N., Telford, O., Teplitz, H.I., Trump, J.R., Vargas, C., Villforth, C., Wagner, C.R., Wandro, P., Wechsler, R.H., Weiner, B.J., Wiklind, T., Wild, V., Wilson, G., Wuyts, S., Yun, M.S.: CANDELS: The Cosmic Assembly Near-infrared Deep Extragalactic Legacy Survey—The Hubble Space Telescope Observations, Imaging Data Products, and Mosaics. Astrophys. J. Suppl. Ser. 197(2), 36 (2011) https://doi.org/10.1088/0067-0049/197/2/36 arXiv:1105.3754 [astro-ph.CO]
- [46] Grogin, N.A., Kocevski, D.D., Faber, S.M., Ferguson, H.C., Koekemoer, A.M., Riess, A.G., Acquaviva, V., Alexander, D.M., Almaini, O., Ashby, M.L.N., Barden, M., Bell, E.F., Bournaud, F., Brown, T.M., Caputi, K.I., Casertano, S., Cassata, P., Castellano, M., Challis, P., Chary, R.-R., Cheung, E., Cirasuolo, M., Conselice, C.J., Roshan Cooray, A., Croton, D.J., Daddi, E., Dahlen, T.,

- Davé, R., de Mello, D.F., Dekel, A., Dickinson, M., Dolch, T., Donley, J.L., Dunlop, J.S., Dutton, A.A., Elbaz, D., Fazio, G.G., Filippenko, A.V., Finkelstein, S.L., Fontana, A., Gardner, J.P., Garnavich, P.M., Gawiser, E., Giavalisco, M., Grazian, A., Guo, Y., Hathi, N.P., Häussler, B., Hopkins, P.F., Huang, J.-S., Huang, K.-H., Jha, S.W., Kartaltepe, J.S., Kirshner, R.P., Koo, D.C., Lai, K., Lee, K.-S., Li, W., Lotz, J.M., Lucas, R.A., Madau, P., McCarthy, P.J., McGrath, E.J., McIntosh, D.H., McLure, R.J., Mobasher, B., Moustakas, L.A., Mozena, M., Nandra, K., Newman, J.A., Niemi, S.-M., Noeske, K.G., Papovich, C.J., Pentericci, L., Pope, A., Primack, J.R., Rajan, A., Ravindranath, S., Reddy, N.A., Renzini, A., Rix, H.-W., Robaina, A.R., Rodney, S.A., Rosario, D.J., Rosati, P., Salimbeni, S., Scarlata, C., Siana, B., Simard, L., Smidt, J., Somerville, R.S., Spinrad, H., Straughn, A.N., Strolger, L.-G., Telford, O., Teplitz, H.I., Trump, J.R., van der Wel, A., Villforth, C., Wechsler, R.H., Weiner, B.J., Wiklind, T., Wild, V., Wilson, G., Wuyts, S., Yan, H.-J., Yun, M.S.: CANDELS: The Cosmic Assembly Near-infrared Deep Extragalactic Legacy Survey. Astrophys. J. Suppl. Ser. 197(2), 35 (2011) https: //doi.org/10.1088/0067-0049/197/2/35 arXiv:1105.3753 [astro-ph.CO]
- [47] de Graaff, A., Brammer, G., Weibel, A., Lewis, Z., Maseda, M.V., Oesch, P.A., Bezanson, R., Boogaard, L.A., Cleri, N.J., Cooper, O.R., Gottumukkala, R., Greene, J.E., Hirschmann, M., Hviding, R.E., Katz, H., Labbé, I., Leja, J., Matthee, J., McConachie, I., Miller, T.B., Naidu, R.P., Price, S.H., Rix, H.-W., Setton, D.J., Suess, K.A., Wang, B., Whitaker, K.E., Williams, C.C.: RUBIES: a complete census of the bright and red distant Universe with JWST/NIRSpec. arXiv e-prints, 2409–05948 (2024) https://doi.org/10.48550/arXiv.2409.05948 arXiv:2409.05948 [astro-ph.GA]
- [48] Brammer, G.: msaexp: NIRSpec analysis tools. Zenodo (2023). https://doi.org/ 10.5281/zenodo.7299500
- [49] Heintz, K.E., Brammer, G.B., Watson, D., Oesch, P.A., Keating, L.C., Hayes, M.J., Abdurro'uf, Arellano-Córdova, K.Z., Carnall, A.C., Christiansen, C.R., Cullen, F., Davé, R., Dayal, P., Ferrara, A., Finlator, K., Fynbo, J.P.U., Flury, S.R., Gelli, V., Gillman, S., Gottumukkala, R., Gould, K., Greve, T.R., Hardin, S.E., Y. -Y Hsiao, T., Hutter, A., Jakobsson, P., Killi, M., Khosravaninezhad, N., Laursen, P., Lee, M.M., Magdis, G.E., Matthee, J., Naidu, R.P., Narayanan, D., Pollock, C., Prescott, M., Rusakov, V., Shuntov, M., Sneppen, A., Smit, R., Tanvir, N.R., Terp, C., Toft, S., Valentino, F., Vijayan, A.P., Weaver, J.R., Wise, J.H., Witstok, J.: The JWST-PRIMAL Legacy Survey. A JWST/NIR-Spec reference sample for the physical properties and Lyman- $\alpha$  absorption and emission of  $\sim 500$  galaxies at z = 5.5 13.4. arXiv e-prints, 2404–02211 (2024) https://doi.org/10.48550/arXiv.2404.02211 arXiv:2404.02211 [astro-ph.GA]
- [50] Horne, K.: An optimal extraction algorithm for CCD spectroscopy. Publ. Astron. Soc. Pac. 98, 609–617 (1986) https://doi.org/10.1086/131801

- [51] Maseda, M.V., Lewis, Z., Matthee, J., Hennawi, J.F., Boogaard, L., Feltre, A., Nanayakkara, T., Bacon, R., Barger, A., Brinchmann, J., Franx, M., Hashimoto, T., Inami, H., Kusakabe, H., Leclercq, F., Rowland, L., Taylor, A.J., Tremonti, C., Urrutia, T., Schaye, J., Simmonds, C., Vitte, E.: JWST/NIRSpec Measurements of Extremely Low Metallicities in High Equivalent Width Lyα Emitters. Astrophys. J. 956(1), 11 (2023) https://doi.org/10.3847/1538-4357/acf12b arXiv:2304.08511 [astro-ph.GA]
- [52] Bagley, M.B., Finkelstein, S.L., Koekemoer, A.M., Ferguson, H.C., Arrabal Haro, P., Dickinson, M., Kartaltepe, J.S., Papovich, C., Pérez-González, P.G., Pirzkal, N., Somerville, R.S., Willmer, C.N.A., Yang, G., Yung, L.Y.A., Fontana, A., Grazian, A., Grogin, N.A., Hirschmann, M., Kewley, L.J., Kirkpatrick, A., Kocevski, D.D., Lotz, J.M., Medrano, A., Morales, A.M., Pentericci, L., Ravindranath, S., Trump, J.R., Wilkins, S.M., Calabrò, A., Cooper, M.C., Costantin, L., de la Vega, A., Hilbert, B., Hutchison, T.A., Larson, R.L., Lucas, R.A., McGrath, E.J., Ryan, R., Wang, X., Wuyts, S.: CEERS Epoch 1 NIRCam Imaging: Reduction Methods and Simulations Enabling Early JWST Science Results. Astrophys. J. Lett. 946(1), 12 (2023) https://doi.org/10.3847/2041-8213/acbb08 arXiv:2211.02495 [astro-ph.IM]
- [53] Brammer, G.: grizli. Zenodo (2023). https://doi.org/10.5281/zenodo.1146904
- [54] Weibel, A., Oesch, P.A., Barrufet, L., Gottumukkala, R., Ellis, R.S., Santini, P., Weaver, J.R., Allen, N., Bouwens, R., Bowler, R.A.A., Brammer, G., Carnall, A.C., Cullen, F., Dayal, P., Donnan, C.T., Dunlop, J.S., Giavalisco, M., Grogin, N.A., Illingworth, G.D., Koekemoer, A.M., Labbe, I., Marchesini, D., McLeod, D.J., McLure, R.J., Naidu, R.P., Shuntov, M., Stefanon, M., Toft, S., Xiao, M.: Galaxy Build-up in the first 1.5 Gyr of Cosmic History: Insights from the Stellar Mass Function at  $z \sim 4-9$  from JWST NIRCam Observations. arXiv e-prints, 2403–08872 (2024) https://doi.org/10.48550/arXiv.2403.08872 arXiv:2403.08872 [astro-ph.GA]
- [55] Bertin, E., Arnouts, S.: SExtractor: Software for source extraction. Astron. Astrophys. Suppl. 117, 393–404 (1996) https://doi.org/10.1051/aas:1996164
- [56] Johnson, B., Leja, J.: Bd-J/Prospector: Initial Release. Zenodo (2017). https://doi.org/10.5281/zenodo.1116491
- [57] Leja, J., Johnson, B.D., Conroy, C., van Dokkum, P.G., Byler, N.: Deriving Physical Properties from Broadband Photometry with Prospector: Description of the Model and a Demonstration of its Accuracy Using 129 Galaxies in the Local Universe. Astrophys. J. 837(2), 170 (2017) https://doi.org/10.3847/1538-4357/aa5ffe arXiv:1609.09073 [astro-ph.GA]
- [58] Conroy, C., Gunn, J.E., White, M.: The Propagation of Uncertainties in Stellar Population Synthesis Modeling. I. The Relevance of Uncertain Aspects of

- Stellar Evolution and the Initial Mass Function to the Derived Physical Properties of Galaxies. Astrophys. J. **699**(1), 486–506 (2009) https://doi.org/10.1088/0004-637X/699/1/486 arXiv:0809.4261 [astro-ph]
- [59] Conroy, C., Gunn, J.E.: The Propagation of Uncertainties in Stellar Population Synthesis Modeling. III. Model Calibration, Comparison, and Evaluation. Astrophys. J. 712(2), 833–857 (2010) https://doi.org/10.1088/0004-637X/712/2/833 arXiv:0911.3151 [astro-ph.CO]
- [60] Sánchez-Blázquez, P., Peletier, R.F., Jiménez-Vicente, J., Cardiel, N., Cenarro, A.J., Falcón-Barroso, J., Gorgas, J., Selam, S., Vazdekis, A.: Medium-resolution Isaac Newton Telescope library of empirical spectra. Mon. Not. R. Astron. Soc. 371(2), 703–718 (2006) https://doi.org/10.1111/j.1365-2966.2006.10699.xarXiv:astro-ph/0607009 [astro-ph]
- [61] Choi, J., Dotter, A., Conroy, C., Cantiello, M., Paxton, B., Johnson, B.D.: Mesa Isochrones and Stellar Tracks (MIST). I. Solar-scaled Models. Astrophys. J. 823(2), 102 (2016) https://doi.org/10.3847/0004-637X/823/2/102 arXiv:1604.08592 [astro-ph.SR]
- [62] Dotter, A.: MESA Isochrones and Stellar Tracks (MIST) 0: Methods for the Construction of Stellar Isochrones. Astrophys. J. Suppl. Ser. 222(1), 8 (2016) https://doi.org/10.3847/0067-0049/222/1/8 arXiv:1601.05144 [astro-ph.SR]
- [63] Chabrier, G.: Galactic Stellar and Substellar Initial Mass Function. Publ. Astron. Soc. Pac. 115(809), 763–795 (2003) https://doi.org/10.1086/376392 arXiv:astro-ph/0304382 [astro-ph]
- [64] Bunker, A.J., Cameron, A.J., Curtis-Lake, E., Jakobsen, P., Carniani, S., Curti, M., Witstok, J., Maiolino, R., D'Eugenio, F., Looser, T.J., Willott, C., Bonaventura, N., Hainline, K., Uebler, H., Willmer, C.N.A., Saxena, A., Smit, R., Alberts, S., Arribas, S., Baker, W.M., Baum, S., Bhatawdekar, R., Bowler, R.A.A., Boyett, K., Charlot, S., Chen, Z., Chevallard, J., Circosta, C., DeCoursey, C., de Graaff, A., Egami, E., Eisenstein, D.J., Endsley, R., Ferruit, P., Giardino, G., Hausen, R., Helton, J.M., Hviding, R.E., Ji, Z., Johnson, B.D., Jones, G.C., Kumari, N., Laseter, I., Luetzgendorf, N., Maseda, M.V., Nelson, E., Parlanti, E., Perna, M., Rawle, T., Rix, H.-W., Rieke, M., Robertson, B., Rodriguez Del Pino, B., Sandles, L., Scholtz, J., Sharpe, K., Skarbinski, M., Stark, D.P., Sun, F., Tacchella, S., Topping, M.W., Villanueva, N.C., Wallace, I.E.B., Williams, C.C., Woodrum, C.: JADES NIRSpec Initial Data Release for the Hubble Ultra Deep Field: Redshifts and Line Fluxes of Distant Galaxies from the Deepest JWST Cycle 1 NIRSpec Multi-Object Spectroscopy. arXiv e-prints, 2306–02467 (2023) https://doi.org/10.48550/arXiv.2306.02467 arXiv:2306.02467 [astro-ph.GA]
- [65] Leja, J., Carnall, A.C., Johnson, B.D., Conroy, C., Speagle, J.S.: How to Measure Galaxy Star Formation Histories. II. Nonparametric Models. Astrophys. J.

- **876**(1), 3 (2019) https://doi.org/10.3847/1538-4357/ab133c arXiv:1811.03637 [astro-ph.GA]
- [66] Kriek, M., Conroy, C.: The Dust Attenuation Law in Distant Galaxies: Evidence for Variation with Spectral Type. Astrophys. J. Lett. 775(1), 16 (2013) https: //doi.org/10.1088/2041-8205/775/1/L16 arXiv:1308.1099 [astro-ph.CO]
- [67] Speagle, J.S.: DYNESTY: a dynamic nested sampling package for estimating Bayesian posteriors and evidences. Mon. Not. R. Astron. Soc. 493(3), 3132–3158 (2020) https://doi.org/10.1093/mnras/staa278 arXiv:1904.02180 [astro-ph.IM]
- [68] Curtis-Lake, E., Carniani, S., Cameron, A., Charlot, S., Jakobsen, P., Maiolino, R., Bunker, A., Witstok, J., Smit, R., Chevallard, J., Willott, C., Ferruit, P., Arribas, S., Bonaventura, N., Curti, M., D'Eugenio, F., Franx, M., Giardino, G., Looser, T.J., Lützgendorf, N., Maseda, M.V., Rawle, T., Rix, H.-W., Rodríguez del Pino, B., Übler, H., Sirianni, M., Dressler, A., Egami, E., Eisenstein, D.J., Endsley, R., Hainline, K., Hausen, R., Johnson, B.D., Rieke, M., Robertson, B., Shivaei, I., Stark, D.P., Tacchella, S., Williams, C.C., Willmer, C.N.A., Bhatawdekar, R., Bowler, R., Boyett, K., Chen, Z., de Graaff, A., Helton, J.M., Hviding, R.E., Jones, G.C., Kumari, N., Lyu, J., Nelson, E., Perna, M., Sandles, L., Saxena, A., Suess, K.A., Sun, F., Topping, M.W., Wallace, I.E.B., Whitler, L.: Spectroscopic confirmation of four metal-poor galaxies at z = 10.3-13.2. Nature Astronomy 7, 622–632 (2023) https://doi.org/10.1038/s41550-023-01918-w arXiv:2212.04568 [astro-ph.GA]
- [69] Leja, J., Johnson, B.D., Conroy, C., van Dokkum, P., Speagle, J.S., Brammer, G., Momcheva, I., Skelton, R., Whitaker, K.E., Franx, M., Nelson, E.J.: An Older, More Quiescent Universe from Panchromatic SED Fitting of the 3D-HST Survey. Astrophys. J. 877(2), 140 (2019) https://doi.org/10.3847/1538-4357/ab1d5a arXiv:1812.05608 [astro-ph.GA]
- [70] Wang, B., Leja, J., Atek, H., Labbé, I., Li, Y., Bezanson, R., Brammer, G., Cutler, S.E., Dayal, P., Furtak, L.J., Greene, J.E., Kokorev, V., Pan, R., Price, S.H., Suess, K.A., Weaver, J.R., Whitaker, K.E., Williams, C.C.: Quantifying the Effects of Known Unknowns on Inferred High-redshift Galaxy Properties: Burstiness, IMF, and Nebular Physics. Astrophys. J. 963(1), 74 (2024) https://doi.org/10.3847/1538-4357/ad187c arXiv:2310.06781 [astro-ph.GA]
- [71] Papovich, C., Finkelstein, S.L., Ferguson, H.C., Lotz, J.M., Giavalisco, M.: The rising star formation histories of distant galaxies and implications for gas accretion with time. Mon. Not. R. Astron. Soc. 412(2), 1123–1136 (2011) https://doi.org/10.1111/j.1365-2966.2010.17965.x arXiv:1007.4554 [astro-ph.CO]
- [72] Behroozi, P., Wechsler, R.H., Hearin, A.P., Conroy, C.: UNIVERSEMACHINE: The correlation between galaxy growth and dark matter halo assembly from z = 0-10. Mon. Not. R. Astron. Soc. **488**(3), 3143–3194 (2019) https://doi.org/10.1093/mnras/stz1182 arXiv:1806.07893 [astro-ph.GA]

- [73] Beverage, A.G., Kriek, M., Suess, K.A., Conroy, C., Price, S.H., Barro, G., Bezanson, R., Franx, M., Lorenz, B., Ma, Y., Mowla, L., Pasha, I., van Dokkum, P., Weisz, D.: The Heavy Metal Survey: The Evolution of Stellar Metallicities, Abundance Ratios, and Ages of Massive Quiescent Galaxies Since z~2. arXiv e-prints, 2312–05307 (2023) https://doi.org/10.48550/arXiv.2312.05307 arXiv:2312.05307 [astro-ph.GA]
- [74] Conroy, C.: Modeling the Panchromatic Spectral Energy Distributions of Galaxies. Annu. Rev. Astron. Astrophys. **51**(1), 393–455 (2013) https://doi.org/10.1146/annurev-astro-082812-141017 arXiv:1301.7095 [astro-ph.CO]
- [75] Whitler, L., Stark, D.P., Endsley, R., Leja, J., Charlot, S., Chevallard, J.: Star formation histories of UV-luminous galaxies at  $z\simeq 6.8$ : implications for stellar mass assembly at early cosmic times. Mon. Not. R. Astron. Soc.  $\bf 519(4)$ , 5859–5881 (2023) https://doi.org/10.1093/mnras/stad004 arXiv:2206.05315 [astro-ph.GA]
- [76] Conroy, C., van Dokkum, P.G.: The Stellar Initial Mass Function in Early-type Galaxies From Absorption Line Spectroscopy. II. Results. Astrophys. J. 760(1), 71 (2012) https://doi.org/10.1088/0004-637X/760/1/71 arXiv:1205.6473 [astro-ph.CO]
- [77] Groves, B.A., Heckman, T.M., Kauffmann, G.: Emission-line diagnostics of low-metallicity active galactic nuclei. Mon. Not. R. Astron. Soc. 371(4), 1559–1569 (2006) https://doi.org/10.1111/j.1365-2966.2006.10812.x arXiv:astro-ph/0607311 [astro-ph]
- [78] de Graaff, A., Rix, H.-W., Carniani, S., Suess, K.A., Charlot, S., Curtis-Lake, E., Arribas, S., Baker, W.M., Boyett, K., Bunker, A.J., Cameron, A.J., Chevallard, J., Curti, M., Eisenstein, D.J., Franx, M., Hainline, K., Hausen, R., Ji, Z., Johnson, B.D., Jones, G.C., Maiolino, R., Maseda, M.V., Nelson, E., Parlanti, E., Rawle, T., Robertson, B., Tacchella, S., Übler, H., Williams, C.C., Willmer, C.N.A., Willott, C.: Ionised gas kinematics and dynamical masses of zrsim6 galaxies from JADES/NIRSpec high-resolution spectroscopy. arXiv e-prints, 2308–09742 (2023) https://doi.org/10.48550/arXiv.2308.09742 arXiv:2308.09742 [astro-ph.GA]
- [79] Wang, B., de Graaff, A., Davies, R.L., Greene, J.E., Leja, J., Goulding, A.D., Williams, C.C., Brammer, G.B., Suess, K.A., Weibel, A., Bezanson, R., Boogaard, L.A., Cleri, N.J., Hirschmann, M., Katz, H., Labbe, I., Maseda, M.V., Matthee, J., McConachie, I., Naidu, R.P., Oesch, P.A., Rix, H.-W., Setton, D.J., Whitaker, K.E.: RUBIES: JWST/NIRSpec Confirmation of an Infrared-luminous, Broad-line Little Red Dot with an Ionized Outflow. arXiv e-prints, 2403–02304 (2024) https://doi.org/10.48550/arXiv.2403.02304 arXiv:2403.02304 [astro-ph.GA]
- [80] Veilleux, S., Osterbrock, D.E.: Spectral Classification of Emission-Line Galaxies.

- [81] Newman, A.B., Belli, S., Ellis, R.S., Patel, S.G.: Resolving Quiescent Galaxies at z ≥ 2. I. Search for Gravitationally Lensed Sources and Characterization of Their Structure, Stellar Populations, and Line Emission. Astrophys. J. 862(2), 125 (2018) https://doi.org/10.3847/1538-4357/aacd4d arXiv:1806.06814 [astro-ph.GA]
- [82] van Dokkum, P.G., Nelson, E.J., Franx, M., Oesch, P., Momcheva, I., Brammer, G., Förster Schreiber, N.M., Skelton, R.E., Whitaker, K.E., van der Wel, A., Bezanson, R., Fumagalli, M., Illingworth, G.D., Kriek, M., Leja, J., Wuyts, S.: Forming Compact Massive Galaxies. Astrophys. J. 813(1), 23 (2015) https://doi.org/10.1088/0004-637X/813/1/23 arXiv:1506.03085 [astro-ph.GA]
- [83] Bezanson, R., van der Wel, A., Straatman, C., Pacifici, C., Wu, P.-F., Barišić, I., Bell, E.F., Conroy, C., D'Eugenio, F., Franx, M., Gallazzi, A., van Houdt, J., Maseda, M.V., Muzzin, A., van de Sande, J., Sobral, D., Spilker, J.: 1D Kinematics from Stars and Ionized Gas at z ~ 0.8 from the LEGA-C Spectroscopic Survey of Massive Galaxies. Astrophys. J. Lett. 868(2), 36 (2018) https://doi.org/10.3847/2041-8213/aaf16b arXiv:1811.07900 [astro-ph.GA]
- [84] Peng, C.Y., Ho, L.C., Impey, C.D., Rix, H.-W.: Detailed Structural Decomposition of Galaxy Images. Astron. J. 124(1), 266–293 (2002) https://doi.org/10.1086/340952 arXiv:astro-ph/0204182 [astro-ph]
- [85] Peng, C.Y., Ho, L.C., Impey, C.D., Rix, H.-W.: Detailed Decomposition of Galaxy Images. II. Beyond Axisymmetric Models. Astron. J. 139(6), 2097–2129 (2010) https://doi.org/10.1088/0004-6256/139/6/2097 arXiv:0912.0731 [astro-ph.CO]
- [86] van der Wel, A., Bell, E.F., Häussler, B., McGrath, E.J., Chang, Y.-Y., Guo, Y., McIntosh, D.H., Rix, H.-W., Barden, M., Cheung, E., Faber, S.M., Ferguson, H.C., Galametz, A., Grogin, N.A., Hartley, W., Kartaltepe, J.S., Kocevski, D.D., Koekemoer, A.M., Lotz, J., Mozena, M., Peth, M.A., Peng, C.Y.: Structural Parameters of Galaxies in CANDELS. Astrophys. J. Suppl. Ser. 203(2), 24 (2012) https://doi.org/10.1088/0067-0049/203/2/24 arXiv:1211.6954 [astro-ph.CO]
- [87] Cutler, S.E., Whitaker, K.E., Weaver, J.R., Wang, B., Pan, R., Bezanson, R., Furtak, L.J., Labbe, I., Leja, J., Price, S.H., Cheng, Y., Clausen, M., Cullen, F., Dayal, P., de Graaff, A., Dickinson, M., Dunlop, J.S., Feldmann, R., Franx, M., Giavalisco, M., Glazebrook, K., Greene, J.E., Grogin, N.A., Illingworth, G., Koekemoer, A.M., Kokorev, V., Marchesini, D., Maseda, M.V., Miller, T.B., Nanayakkara, T., Nelson, E.J., Setton, D.J., Shipley, H., Suess, K.A.: Two Distinct Classes of Quiescent Galaxies at Cosmic Noon Revealed by JWST PRIMER and UNCOVER. arXiv e-prints, 2312–15012 (2023) https://doi.org/10.48550/arXiv.2312.15012 arXiv:2312.15012 [astro-ph.GA]

- [88] Szomoru, D., Franx, M., van Dokkum, P.G., Trenti, M., Illingworth, G.D., Labbé, I., Bouwens, R.J., Oesch, P.A., Carollo, C.M.: Confirmation of the Compactness of a z = 1.91 Quiescent Galaxy with Hubble Space Telescope's Wide Field Camera 3. Astrophys. J. Lett. 714(2), 244–248 (2010) https://doi.org/10.1088/2041-8205/714/2/L244 arXiv:1004.1411 [astro-ph.CO]
- [89] Ito, K., Valentino, F., Brammer, G., Faisst, A.L., Gillman, S., Gomez-Guijarro, C., Gould, K.M.L., Heintz, K.E., Ilbert, O., Kragh Jespersen, C., Kokorev, V., Kubo, M., Magdis, G.E., McPartland, C., Onodera, M., Rizzo, F., Tanaka, M., Toft, S., Vijayan, A.P., Weaver, J.R., Whitaker, K.E., Wright, L.: Size Stellar Mass Relation and Morphology of Quiescent Galaxies at z ≥ 3 in Public JWST Fields. arXiv e-prints, 2307–06994 (2023) https://doi.org/10.48550/arXiv.2307.06994 arXiv:2307.06994 [astro-ph.GA]
- [90] Suess, K.A., Kriek, M., Price, S.H., Barro, G.: Color Gradients along the Quiescent Galaxy Sequence: Clues to Quenching and Structural Growth. Astrophys. J. Lett. 899(2), 26 (2020) https://doi.org/10.3847/2041-8213/abacc9 arXiv:2008.02817 [astro-ph.GA]
- [91] Harikane, Y., Ouchi, M., Ono, Y., Fujimoto, S., Donevski, D., Shibuya, T., Faisst, A.L., Goto, T., Hatsukade, B., Kashikawa, N., Kohno, K., Hashimoto, T., Higuchi, R., Inoue, A.K., Lin, Y.-T., Martin, C.L., Overzier, R., Smail, I., Toshikawa, J., Umehata, H., Ao, Y., Chapman, S., Clements, D.L., Im, M., Jing, Y., Kawaguchi, T., Lee, C.-H., Lee, M.M., Lin, L., Matsuoka, Y., Marinello, M., Nagao, T., Onodera, M., Toft, S., Wang, W.-H.: SILVERRUSH. VIII. Spectroscopic Identifications of Early Large-scale Structures with Protoclusters over 200 Mpc at z ~ 6-7: Strong Associations of Dusty Star-forming Galaxies. Astrophys. J. 883(2), 142 (2019) https://doi.org/10.3847/1538-4357/ab2cd5 arXiv:1902.09555 [astro-ph.GA]
- [92] Maseda, M.V., de Graaff, A., Franx, M., Rix, H.-W., Carniani, S., Laseter, I., Dudzeviciute, U., Rawle, T., Parlanti, E., Arribas, S., Bunker, A.J., Cameron, A.J., Charlot, S., Curti, M., D'Eugenio, F., Jones, G.C., Kumari, N., Maiolino, R., Uebler, H., Saxena, A., Smit, R., Willott, C., Witstok, J.: The NIRSpec Wide GTO Survey. arXiv e-prints, 2403–05506 (2024) https://doi.org/10.48550/arXiv.2403.05506 arXiv:2403.05506 [astro-ph.GA]
- [93] Nakajima, K., Ouchi, M., Isobe, Y., Harikane, Y., Zhang, Y., Ono, Y., Umeda, H., Oguri, M.: JWST Census for the Mass-Metallicity Star Formation Relations at z = 4-10 with Self-consistent Flux Calibration and Proper Metallicity Calibrators. Astrophys. J. Suppl. Ser. 269(2), 33 (2023) https://doi.org/10.3847/1538-4365/acd556 arXiv:2301.12825 [astro-ph.GA]
- [94] Zavala, J.A., Buat, V., Casey, C.M., Finkelstein, S.L., Burgarella, D., Bagley, M.B., Ciesla, L., Daddi, E., Dickinson, M., Ferguson, H.C., Franco, M., Jiménez-Andrade, E.F., Kartaltepe, J.S., Koekemoer, A.M., Le Bail, A., Murphy, E.J.,

- Papovich, C., Tacchella, S., Wilkins, S.M., Aretxaga, I., Behroozi, P., Champagne, J.B., Fontana, A., Giavalisco, M., Grazian, A., Grogin, N.A., Kewley, L.J., Kocevski, D.D., Kirkpatrick, A., Lotz, J.M., Pentericci, L., Pérez-González, P.G., Pirzkal, N., Ravindranath, S., Somerville, R.S., Trump, J.R., Yang, G., Yung, L.Y.A., Almaini, O., Amorín, R.O., Annunziatella, M., Arrabal Haro, P., Backhaus, B.E., Barro, G., Bell, E.F., Bhatawdekar, R., Bisigello, L., Buitrago, F., Calabrò, A., Castellano, M., Chávez Ortiz, Ó.A., Chworowsky, K., Cleri, N.J., Cohen, S.H., Cole, J.W., Cooke, K.C., Cooper, M.C., Cooray, A.R., Costantin, L., Cox, I.G., Croton, D., Davé, R., de La Vega, A., Dekel, A., Elbaz, D., Estrada-Carpenter, V., Fernández, V., Finkelstein, K.D., Freundlich, J., Fujimoto, S., García-Argumánez, A., Gardner, J.P., Gawiser, E., Gómez-Guijarro, C., Guo, Y., Hamilton, T.S., Hathi, N.P., Holwerda, B.W., Hirschmann, M., Huertas-Company, M., Hutchison, T.A., Iyer, K.G., Jaskot, A.E., Jha, S.W., Jogee, S., Juneau, S., Jung, I., Kassin, S.A., Kurczynski, P., Larson, R.L., Leung, G.C.K., Long, A.S., Lucas, R.A., Magnelli, B., Mantha, K.B., Matharu, J., McGrath, E.J., McIntosh, D.H., Medrano, A., Merlin, E., Mobasher, B., Morales, A.M., Newman, J.A., Nicholls, D.C., Pandya, V., Rafelski, M., Ronayne, K., Rose, C., Ryan, R.E., Santini, P., Seillé, L.-M., Shah, E.A., Shen, L., Simons, R.C., Snyder, G.F., Stanway, E.R., Straughn, A.N., Teplitz, H.I., Vanderhoof, B.N., Vega-Ferrero, J., Wang, W., Weiner, B.J., Willmer, C.N.A., Wuyts, S., Ceers Team: Dusty Starbursts Masquerading as Ultra-high Redshift Galaxies in JWST CEERS Observations. Astrophys. J. Lett. 943(2), 9 (2023) https://doi.org/10.3847/2041-8213/acacfe arXiv:2208.01816 [astro-ph.GA]
- [95] Vijayan, A.P., Lovell, C.C., Wilkins, S.M., Thomas, P.A., Barnes, D.J., Irodotou, D., Kuusisto, J., Roper, W.J.: First Light And Reionization Epoch Simulations (FLARES) II: The photometric properties of high-redshift galaxies. Mon. Not. R. Astron. Soc. 501(3), 3289–3308 (2021) https://doi.org/10.1093/mnras/staa3715 arXiv:2008.06057 [astro-ph.GA]
- [96] Lovell, C.C., Vijayan, A.P., Thomas, P.A., Wilkins, S.M., Barnes, D.J., Irodotou, D., Roper, W.: First Light And Reionization Epoch Simulations (FLARES) I. Environmental dependence of high-redshift galaxy evolution. Mon. Not. R. Astron. Soc. 500(2), 2127–2145 (2021) https://doi.org/10.1093/mnras/staa3360arXiv:2004.07283 [astro-ph.GA]
- [97] Crain, R.A., Schaye, J., Bower, R.G., Furlong, M., Schaller, M., Theuns, T., Dalla Vecchia, C., Frenk, C.S., McCarthy, I.G., Helly, J.C., Jenkins, A., Rosas-Guevara, Y.M., White, S.D.M., Trayford, J.W.: The EAGLE simulations of galaxy formation: calibration of subgrid physics and model variations. Mon. Not. R. Astron. Soc. 450(2), 1937–1961 (2015) https://doi.org/10.1093/mnras/stv725 arXiv:1501.01311 [astro-ph.GA]
- [98] Schaye, J., Crain, R.A., Bower, R.G., Furlong, M., Schaller, M., Theuns, T., Dalla Vecchia, C., Frenk, C.S., McCarthy, I.G., Helly, J.C., Jenkins, A., Rosas-Guevara, Y.M., White, S.D.M., Baes, M., Booth, C.M., Camps, P., Navarro,

- J.F., Qu, Y., Rahmati, A., Sawala, T., Thomas, P.A., Trayford, J.: The EAGLE project: simulating the evolution and assembly of galaxies and their environments. Mon. Not. R. Astron. Soc. **446**(1), 521–554 (2015) https://doi.org/10.1093/mnras/stu2058 arXiv:1407.7040 [astro-ph.GA]
- [99] Nelson, D., Pillepich, A., Springel, V., Weinberger, R., Hernquist, L., Pakmor, R., Genel, S., Torrey, P., Vogelsberger, M., Kauffmann, G., Marinacci, F., Naiman, J.: First results from the IllustrisTNG simulations: the galaxy colour bimodality. Mon. Not. R. Astron. Soc. 475(1), 624–647 (2018) https://doi.org/10.1093/mnras/stx3040 arXiv:1707.03395 [astro-ph.GA]
- [100] Nelson, D., Springel, V., Pillepich, A., Rodriguez-Gomez, V., Torrey, P., Genel, S., Vogelsberger, M., Pakmor, R., Marinacci, F., Weinberger, R., Kelley, L., Lovell, M., Diemer, B., Hernquist, L.: The IllustrisTNG simulations: public data release. Computational Astrophysics and Cosmology 6(1), 2 (2019) https://doi.org/10.1186/s40668-019-0028-x arXiv:1812.05609 [astro-ph.GA]
- [101] Pillepich, A., Nelson, D., Hernquist, L., Springel, V., Pakmor, R., Torrey, P., Weinberger, R., Genel, S., Naiman, J.P., Marinacci, F., Vogelsberger, M.: First results from the IllustrisTNG simulations: the stellar mass content of groups and clusters of galaxies. Mon. Not. R. Astron. Soc. 475(1), 648–675 (2018) https://doi.org/10.1093/mnras/stx3112 arXiv:1707.03406 [astro-ph.GA]
- [102] Springel, V., Pakmor, R., Pillepich, A., Weinberger, R., Nelson, D., Hernquist, L., Vogelsberger, M., Genel, S., Torrey, P., Marinacci, F., Naiman, J.: First results from the illustristing simulations: matter and galaxy clustering. Monthly Notices of the Royal Astronomical Society 475(1), 676–698 (2017) https://doi.org/10.1093/mnras/stx3304
- [103] Marinacci, F., Vogelsberger, M., Pakmor, R., Torrey, P., Springel, V., Hernquist, L., Nelson, D., Weinberger, R., Pillepich, A., Naiman, J., Genel, S.: First results from the illustristing simulations: radio haloes and magnetic fields. Monthly Notices of the Royal Astronomical Society (2018) https://doi.org/10.1093/mnras/sty2206
- [104] Naiman, J.P., Pillepich, A., Springel, V., Ramirez-Ruiz, E., Torrey, P., Vogelsberger, M., Pakmor, R., Nelson, D., Marinacci, F., Hernquist, L., Weinberger, R., Genel, S.: First results from the illustristing simulations: a tale of two elements chemical evolution of magnesium and europium. Monthly Notices of the Royal Astronomical Society 477(1), 1206–1224 (2018) https://doi.org/10.1093/mnras/sty618
- [105] Hirschmann, M., De Lucia, G., Fontanot, F.: Galaxy assembly, stellar feedback and metal enrichment: the view from the GAEA model. Mon. Not. R. Astron. Soc. 461(2), 1760–1785 (2016) https://doi.org/10.1093/mnras/stw1318 arXiv:1512.04531 [astro-ph.GA]

- [106] Fontanot, F., De Lucia, G., Hirschmann, M., Xie, L., Monaco, P., Menci, N., Fiore, F., Feruglio, C., Cristiani, S., Shankar, F.: The rise of active galactic nuclei in the galaxy evolution and assembly semi-analytic model. Mon. Not. R. Astron. Soc. 496(3), 3943–3960 (2020) https://doi.org/10.1093/mnras/staa1716arXiv:2002.10576 [astro-ph.CO]
- [107] Xie, L., De Lucia, G., Hirschmann, M., Fontanot, F.: The influence of environment on satellite galaxies in the GAEA semi-analytic model. Mon. Not. R. Astron. Soc. 498(3), 4327–4344 (2020) https://doi.org/10.1093/mnras/staa2370 arXiv:2003.12757 [astro-ph.GA]
- [108] Springel, V., White, S.D.M., Jenkins, A., Frenk, C.S., Yoshida, N., Gao, L., Navarro, J., Thacker, R., Croton, D., Helly, J., Peacock, J.A., Cole, S., Thomas, P., Couchman, H., Evrard, A., Colberg, J., Pearce, F.: Simulations of the formation, evolution and clustering of galaxies and quasars. Nature 435(7042), 629–636 (2005) https://doi.org/10.1038/nature03597 arXiv:astro-ph/0504097 [astro-ph]
- [109] Elahi, P.J., Welker, C., Power, C., Lagos, C.d.P., Robotham, A.S.G., Cañas, R., Poulton, R.: SURFS: Riding the waves with Synthetic UniveRses For Surveys. Mon. Not. R. Astron. Soc. 475(4), 5338–5359 (2018) https://doi.org/10.1093/mnras/sty061 arXiv:1712.01988 [astro-ph.GA]
- [110] Solanes, J.M., Perea, J.D., Valentí-Rojas, G.: Timescales of major mergers from simulations of isolated binary galaxy collisions. Astron. Astrophys. 614, 66 (2018) https://doi.org/10.1051/0004-6361/201832855 arXiv:1804.10559 [astro-ph.GA]
- [111] Kennicutt, R.C., Evans, N.J.: Star Formation in the Milky Way and Nearby Galaxies. Annu. Rev. Astron. Astrophys. **50**, 531–608 (2012) https://doi.org/10.1146/annurev-astro-081811-125610 arXiv:1204.3552 [astro-ph.GA]